Cell Reports
Medicine

Article

A combined "eat me/don't eat me" strategy based on exosome for acute liver injury treatment

Graphical abstract

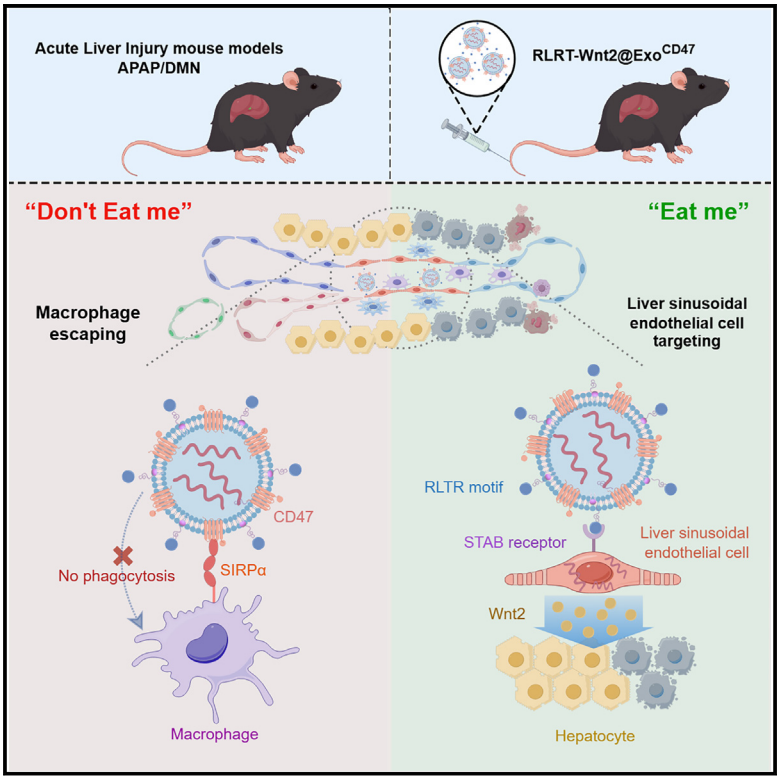

Highlights

- RLTRKRGLK surface modification enables LSEC-targeted exosome delivery
- CD47 engineering reduces macrophage clearance via "don't eat me" signaling
- RLTR-Wnt2@Exo^{CD47} attenuates liver necrosis and enhances regeneration

Authors

Wei Du, Chen Chen, YingYing Liu, ..., JuanLi Duan, Fei He, Lin Wang

Correspondence

duan_juan_li@126.com (J.D.),
hefei_hefei@163.com (F.H.),
fierywang@163.com (L.W.)

In brief

Du et al. develop an exosome-based dual-targeting platform integrating "eat me/don't eat me" strategies. By combining LSEC-directed RLTRKRGLK ligand display with CD47-mediated phagocytic evasion, this system enables precise Wnt2 mRNA delivery to liver sinusoidal endothelia, effectively ameliorating drug-induced acute liver injury and enhancing hepatic regeneration.

Du et al., 2025, Cell Reports Medicine 6, 102033
April 15, 2025
https://doi.org/10.1016/j.xcrm.2025.102033

CellPress

Cell Reports Medicine

CellPress
OPEN ACCESS

Article

A combined "eat me/don't eat me" strategy based on exosome for acute liver injury treatment

Wei Du,[1,3] Chen Chen,[1,3] YingYing Liu,[1,3] Huiyi Quan,[2] Ming Xu,[1] JingJing Liu,[1] Ping Song,[1] ZhiQiang Fang,[1] ZhenSheng Yue,[1] Hao Xu,[1] YuWei Ling,[1] JuanLi Duan,[1,*] Fei He,[1,*] and Lin Wang[1,4,*]

[1]Department of Hepatobiliary Surgery, Xijing Hospital, Fourth Military Medical University, Xi'an 710032, China
[2]Department of Dermatology, Xijing Hospital, Fourth Military Medical University, Xi'an 710032, China
[3]These authors contributed equally
[4]Lead contact
*Correspondence: duan_juan_li@126.com (J.D.), hefei_hefei@163.com (F.H.), fierywang@163.com (L.W.)
https://doi.org/10.1016/j.xcrm.2025.102033

SUMMARY

Drug-induced liver injury (DILI) involves multifaceted pathogenesis, necessitating effective therapeutic strategies. Wnt2, secreted by liver sinusoidal endothelial cell (LSEC), activates the Wnt/β-catenin signaling pathway to promote hepatocyte proliferation after injury. To address the dual challenges of targeted delivery and phagocytosis evasion, we develop a combined "eat me/don't eat me" strategy. RLTRKRGLK (RLTR) peptide-functionalized exosomes are engineered by inserting DMPE-PEG2000-CRLTRKRGLK into the lipid membrane of exosome derived from bEnd.3 cell. Surface-displayed RLTR mediates exosomal enrichment in LSEC, while CD47 engineering reduces macrophage clearance via "don't eat me" signaling. Then, lentiviral transfection enables stable encapsulation of functional Wnt2 mRNA into Exo^{CD47} (designated Wnt2@Exo^{CD47}). In both acetaminophen (APAP) and dimethylnitrosamine (DMN)-induced murine liver injury models, RLTR-Wnt2@Exo^{CD47} demonstrates LSEC-specific targeting and significant hepatoprotection. This engineered exosome platform provides a therapeutic strategy for DILI.

INTRODUCTION

As the largest solid organ, the liver serves as the primary metabolic hub for xenobiotic processing, making drug-induced liver injury a critical bottleneck in pharmaceutical development and clinical translation.[1] The mechanism underlying DILI is intricate, and effective treatment strategies are lacking.[2,3] Often overlooked is the presence of a significant population of non-parenchymal cells (NPCs) in the liver, among which liver sinusoidal endothelial cells are the most abundant. The unique fenestrated architecture and paracrine signaling capacity position them as key regulators in hepatic pathophysiology, and DILI is no exception.[4] Crucially, these cells secrete angiocrine factors essential for liver regeneration, including Wnt9b (predominantly expressed by central venous endothelial cells) and Wnt2 (expressed by both central venous and sinusoidal endothelial populations), highlighting LSEC as a potential therapeutic target.[5–7] The Wnt2 signaling axis, through binding to Frizzled (FZD) receptors and low-density lipoprotein receptor-related protein 5/6 (LRP5/6) co-receptors, triggers a canonical signaling cascade involving the following: dissociation of the β-catenin destruction complex, enabling cytoplasmic β-catenin stabilization; nuclear translocation of β-catenin, which activates proliferation-associated genes; and dual stimulation of mature hepatocyte proliferation and hepatic progenitor cell differentiation. These mechanisms collectively establish Wnt2 as a master regulator of hepatic repair processes.[8,9]

Exosomes, naturally secreted phospholipid bilayer nanovesicles, exhibit superior biocompatibility and lower immunogenicity compared to artificial nanocarriers. More importantly, the engineering of exosomes for targeted therapeutic delivery have significantly augmented their translational potential in the realm of precision medicine.[10] Strategic modifications of exosome membranes via amphiphilic molecule integration, combined with payload encapsulation of bioactive compounds, enable cell-specific targeting capabilities.[11] Chemical engineering approaches, particularly the integration of amphiphilic molecules into the exosomal lipid bilayer, provide a robust method for exosome engineering. 1,2-Dimyristoyl-*sn*-glycero-3-phosphoethanolamine-polyethylene glycol 2000 (DMPE-PEG2000) is an amphiphilic molecule widely used to carry functional ligands to achieve targeted modification of exosomes.[12] Notably, peptide-modified nanocarriers featuring the RXR/RXXR motif from Apolipoprotein B-100 (ApoB-100) have demonstrated selective binding to Stabilin2 (STAB2) receptor expressed on LSEC, enhancing endocytic uptake for precision therapy in LSEC-associated pathologies.[13] Despite these advances, the development of LSEC-targeted exosome delivery systems remains unexplored.

An ideal nanocarrier must maintain biological stability in the complex system, exhibit prolonged circulation half-life for enhanced target accumulation, and evade the mononuclear phagocyte system (MPS). Current exosome-based delivery systems face significant challenges, with the majority of the administered dose typically sequestered by MPS, compromising

therapeutic efficacy and potentially inducing off-target toxicity.[14] CD47, known as the "don't eat me" signal, has emerged as a key biological checkpoint regulating phagocytic clearance.[15] Extensive research has elucidated the mechanistic involvement of CD47 in tumorigenesis. Elevated CD47 expression on malignant cell surfaces reduces their susceptibility to immune detection, thereby promoting tumor immune evasion through suppression of phagocytic clearance and dysregulation of adaptive immune responses.[16] CD47 interacts with signal regulatory protein alpha (SIRPa), which is highly expressed on macrophages, to inhibit macrophage-mediated phagocytosis through the CD47-SIRPa axis, effectively sending a "don't eat me" signal.[17–19] This interaction has inspired the development of nanoparticles coated with CD47 or its derived peptides, which significantly impede their engulfment by macrophages, thereby enhancing the targeted delivery of therapeutic agents to specific organs or tissues.

Accordingly, we have developed an exosome-based "eat me/don't eat me" strategy that combines dual-targeting effects to minimize exosome sequestration by macrophage and enhance the LSEC targeting. We functionalized the exosomes from bEnd.3 with DMPE-PEG2000-CRLTRKRGLK to bolster their LSEC-targeting capability; the resulting RLTR-modified exosomes (designated RLTR-Exo) are responsible for the "eat me" tactic. Conversely, the subsequent "don't eat me" signal was achieved by using CD47 engineering exosomes originating from $CD47^{OE}$-bEnd.3, which further diminishes exosomes clearance by the MPS. Furthermore, therapeutic nucleic acid drugs (Wnt2 mRNA) were loaded into the exosomes by Wnt2 lentiviral transfection, and the drug delivery system was named RLTR-Wnt2@Exo^{CD47}. Interestingly, this strategy effectively minimizes exosome sequestration by the MPS, enhances LSEC accumulation, and improves the therapeutic outcomes for liver injury in mice without adverse effects.

RESULTS

Synthesis and characterization of RLTR-Exo

Exosome (Exo) was isolated from the culture medium of bEnd.3 cells. Transmission electron microscopy (TEM) analysis revealed that Exo was a spherical vesicle with a bilayer membrane structure (Figure 1A). The nanoparticle tracking analysis (NTA) detection results show that the particle size of bEnd.3-Exo was mainly distributed in the range of 40–200 nm, with the peak at 117.9 nm (Figure 1B). Western blotting analysis confirmed the expression of exosomal marker protein, including Alix, TSG101, and Flotillin1, whereas the expression of mitochondrial membrane protein VDAC1 was barely detectable (Figure 1C).

In this study, CRLTRKRGLK was conjugated to DMPE-PEG2000-Mal via a thiol-maleimide reaction. The chemical structural formula and ^{1}H NMR spectrum of the product (DMPE-PEG2000-CRLTRKRGLK) were shown in Figures 1D and 1E, demonstrating successful covalent linkage. For exosome surface functionalization, DMPE-PEG2000-CRLTRK RGLK (RLTR) was incorporated into exosomal membranes through hydrophobic insertion of the DMPE moiety during 1 h incubation at 40°C (Figure 1F). TEM analysis confirmed that RLTR-Exo retained native spherical morphology and bilayer membrane integrity, indistinguishable from unmodified exosomes (Exo), as indicated by the black arrows in Figure 1G. To quantitatively assess surface modification, DMPE-PEG2000-CRLTRKRGLK conjugated with fluorescein isothiocyanate (FITC) was synthesized. The particle size distribution of Exo and RLTR-Exo together with the modification efficiency was determined through nanoflow cytometry (NanoFCM). RLTR-Exo exhibited a modest diameter increase from 67.8 (Exo) to 74.8 (RLTR-Exo), while maintaining a size distribution (40–200 nm) consistent with exosome definitions. Unlike the Exo group, it could also be observed that there were two main peaks in the particle size distribution of the RLTR-Exo group, indicating the heterogeneity of the particles in the RLTR-Exo group (Figure 1H). Critically, 87.5% of RLTR-Exo demonstrated FITC fluorescence by NanoFCM (Figure 1I), confirming efficient surface modification. Collectively, these results demonstrated that exosome derived from bEnd.3 cells was successfully isolated and modified with RLTR.

RLTR surface modification enhances exosome uptake by LSEC

To investigate whether the surface modification of exosome with RLTR would enhance the cellular uptake of exosome by mouse primary LSEC *in vitro*, LSEC was isolated and cultured on cover slides in 24-well plates. To visualize the internalization of exosome, Exo and RLTR-Exo were labeled with 3,3'-dioctadecyloxacarbocyanine perchlorate (DiO) in the dark and then incubated with LSEC for 30 min. Confocal laser scanning microscopy (CLSM) images showed that both of Exo and RLTR-Exo were successfully phagocytized by LSEC. Using unmodified Exo as control, a significantly higher DiO fluorescence intensity was observed in the RLTR-Exo group (Figure 2A). Additionally, to evaluate the binding effect of RLTR-Exo, Exo and RLTR-Exo were labeled with 1,1'-dioctadecyl-3,3,3',3'-tetramethylindocarbocyanine perchlorate (DiI) and then incubated with primary LSEC in dark for 30 min. The fluorescence radiation efficiency of cell culture slides in the RLTR-Exo group was significantly higher compared to the Exo group, which was consistent with the results observed by confocal microscopy (Figure 2B). The aforementioned results indicate that the surface modification with RLTR peptides obviously enhanced the binding ability of exosome to LSEC *in vitro*.

To assess whether the improved organ distribution and the membrane modification resulted in improved half-life of exosome in the liver, we next conducted a comprehensive analysis to determine the systemic distribution and pharmacokinetic properties of exosome in mice. In Figure 2C, we employed serial *ex vivo* organs distribution fluorescence imaging of DiI-labeled exosome injected intravenously in mice over a 14 days period. The results showed that membrane modification of RLTR significantly promoted the enrichment of exosome in the mouse liver, while reducing their residence in the lungs. In Figure 2D, we quantitatively analyzed the temporal dynamics of exosome distribution in the liver. Fluorescence imaging confirmed similar DiI signal between Exo and RLTR-Exo for the first 12 h after injection. However, the RLTR-Exo group had significantly higher fluorescence signal at day 3 and at day 5, lasting up to day 7 after injection. The half-life of Exo in the liver was found to be 3 days, while the half-life of RLTR-Exo is extended to 9 days. Taken together, these

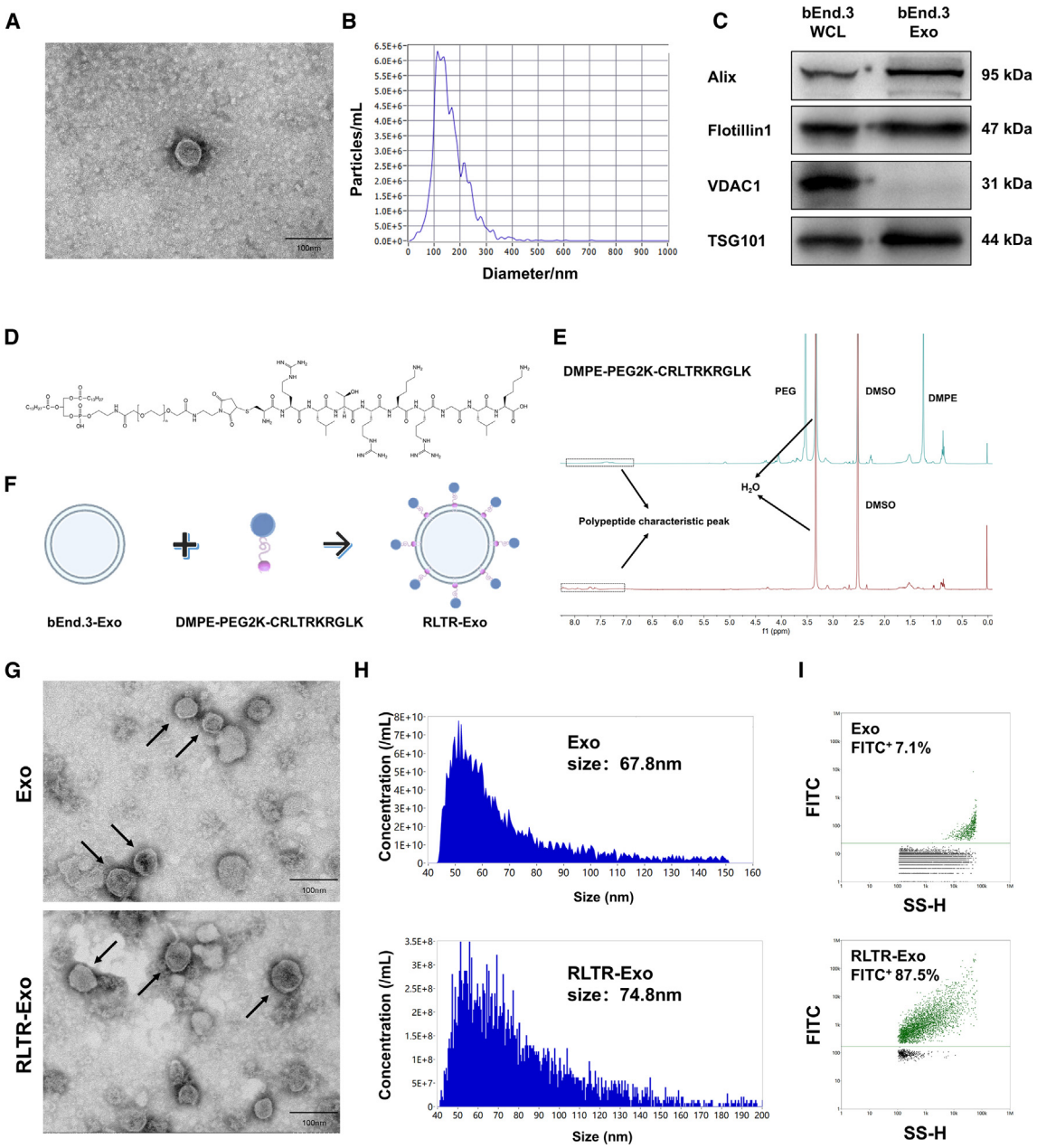

Figure 1. Synthesis and characterization of RLTR-Exo

(A and B) TEM image and NTA for size of exosomes isolated from bEnd.3. Scale bar: 200 nm.
(C) Western blotting (WB) for Alix, Flotillin1, VDAC1, and TSG101.
(D) Chemical structural formula of DMPE-PEG2000-CRLTRKRGLK.
(E) ^{1}H NMR spectrum of DMPE-PEG2000-CRLTRKRGLK and CRLTRKRGLK.
(F) Schematic illustration of the procedure to produce engineered exosome (RLTR-Exo).
(G) TEM images of Exo and RLTR-Exo.
(H) Particle size distributions of Exo and RLTR-Exo measured by NanoFCM.
(I) Modification efficiency of RLTR-Exo detected via NanoFCM.

findings indicate that RLTR surface modification improves long-term retainment of exosome in the liver.

To confirm that the distribution of RLTR-Exo in LSEC was due to RLTR peptide-specific targeting of LSEC, we used flow cytometry (FCM) to analyze the uptake of RLTR-Exo by the NPCs in the liver, especially LSECs and Kupffer cells (KCs). Primary NPCs were isolated after single injection with DiO-labeled Exo or RLTR-Exo, and the ratio of DiO^{+} LSEC/KC in NPCs was

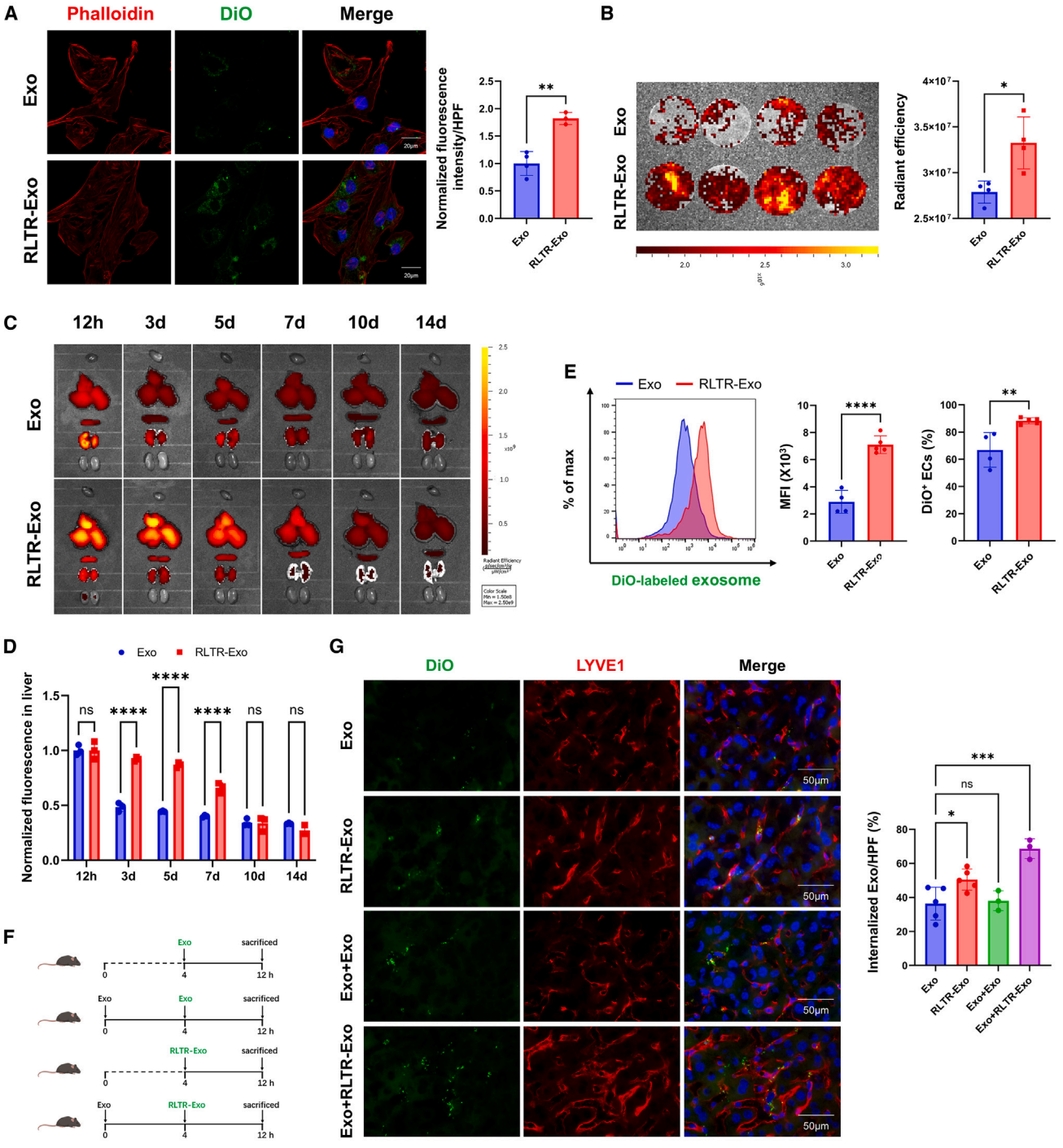

Figure 2. RLTR peptide surface modification enhances exosome uptake by LSEC *in vitro* and *in vivo*

(A) CLSM images showing internalization of Exo and RLTR-Exo by primary LSEC *in vitro* and quantitative analysis of the DiO fluorescence intensity. Red: TRITC-phalloidin labeled F-actin. Green: DiO-labeled Exo and RLTR-Exo. Blue: DAPI labeled nuclei. Exo: $n = 4$, RLTR-Exo: $n = 3$. Scale bar: 20 μm.

(B) *Ex vivo* fluorescence images showing the retention of DiI-labeled Exo (up) and RLTR-Exo (down) in primary LSEC 0.5 h after incubation and quantitative analysis of the radiant efficiency of *ex vivo* images.

(C) *Ex vivo* fluorescence images of main organs treated with DiI-labeled Exo or DiI-labeled RLTR-Exo on day 0.5, 3, 5, 7, 10, and 14 after administration ($n = 3$ for all groups).

(D) Quantification of fluorescence intensity over the 14-day treatment period. Data are normalized to the fluorescence intensity at 12 h.

(legend continued on next page)

analyzed through FCM. LSECs were defined as $CD31^+$ cells, while KCs were defined as $F4/80^+$ cells; the gating strategies are shown in Figure S1A. Figure 2E showed representative FCM histograms for the fluorescent intensity of DiO-labeled exosome within the LSECs in the liver. The quantificational data of the mean fluorescence intensity (MFI) revealed that the ability to uptake RLTR-Exo is higher than Exo in LSECs, and the RLTR surface modification significantly increased the ratio of DiO^+ endothelial cells (ECs) and DiO^+ NPCs (Figure S1B). Additionally, we also observed strong non-specific phagocytosis of Exo and RLTR-Exo by KCs in the liver. FCM analysis revealed that the RLTR modification on the exosome surface did not substantially alter the percentage of DiO^+ KCs. These observations indicated that the surface modification with the RLTR peptides markedly enhanced the internalization of RLTR-Exo by LSEC *in vivo*.

Notably, we found it difficult to remove the cellular uptake of exosome by KC in the liver. Therefore, we designed the sequential injection strategies to eliminate interference from the MPS and more directly evaluated the improvement on LSEC-targeting ability of exosomes with RLTR modification. Different from the single-injection strategies, the sequential strategies were achieved first injecting exosome without any modification via the tail vein to saturate the macrophages prior to the administration of the second injection, thereby minimizing its noise by the MPS. According to the previous study,[14] we chose 4 h as the time interval between the two dosing in the following study (Figure 2F). To explore the distribution of DiO-labeled exosomes *in vivo*, we collected the main organs (including the heart, liver, spleen, lung, and kidney) from mice injected with different formulations for frozen sections. The immunofluorescence staining revealed that the DiO-labeled exosomes, after being injected into mice, primarily accumulated in the liver, with smaller quantities observed in the spleen and lungs (Figure S1C). Next, we used LYVE1 to label LSEC and F4/80 to label KCs in frozen liver sections to analyze the co-localization of DiO-labeled exosomes and LSEC or KC through immunofluorescence. The comparison of LSEC accumulation of exosome across different injection strategies revealed that RLTR-Exo exhibited significantly higher enrichment in LSEC than Exo, which is consistent with the results of FCM. Furthermore, the sequential treatment obviously promoted LSEC to internalize more RLTR-Exo compared to single-injection strategies (Figure 2G). Consequently, the Exo + RLTR-Exo group exhibited the highest distribution of DiO-labeled exosomes in LSEC. It was noteworthy that pretreatment of Exo resulted in a significantly fewer distribution of RLTR-Exo in KC (Figure S1D). These results could be attributed to the MPS blockade by unmodified Exo and ligand-mediated delivery due to RLTR conjugation. However, the sequential strategies exhibited limited efficacy in inhibiting the non-specific phagocytosis of macrophages. Consequently, there is a need to explore more effective methods to counteract macrophage phagocytosis.

CD47 engineering exosome escapes the phagocytosis by macrophage

To functionalize the Exo with CD47 on the surface, the donor cells (bEnd.3) were transfected with CD47-overexpressing lentivirus. Exosomes were isolated from the culture medium of CD47-overexpressing bEnd.3 cells ($CD47^{OE}$-bEnd.3); western blot analysis showed the positive expression of exosomal markers TSG101, Flotillin1, and Alix in both Exo and Exo^{CD47}, while VDAC1 was not found in both. Moreover, CD47 protein level was significantly higher in Exo^{CD47} than that in control Exo (Figures 3A and S2). Immunogold transmission electron microscopy (IG-TEM) revealed that CD47 protein in the Exo^{CD47} was more extensively anchored to the membrane than Exo (Figure 3B). Gold particles conjugated with secondary antibody may destroy the membrane structure of exosomes. However, a clear increase in the number of gold particles adhering to the Exo^{CD47} membrane was observed. Furthermore ELISA, which precisely measures the content of CD47 in exosomes, showed higher CD47 expression in Exo^{CD47} than Exo (Figure 3C). In summary, these data confirmed the exosome feature of Exo^{CD47}.

To explore whether Exo^{CD47} could escape the macrophage phagocytosis, RAW264.7 cells culture slides were prepared, and DiO-labeled Exo and Exo^{CD47} were incubated with RAW264.7 in the dark. CLSM images showed significantly reduced fluorescence intensity of DiO in the Exo^{CD47} group compared to the Exo group (Figure 3D). RAW264.7 was counted and cultured on cover glass slides in a 24-well plate. DiI-labeled Exo and Exo^{CD47} were incubated with RAW264.7 for 1 h; fluorescence imaging showed significantly less Exo^{CD47} phagocytosed by RAW264.7 cells than Exo (Figure 3E). Exo and Exo^{CD47} were labeled with DiO and then incubated with RAW264.7 in the dark for 1 h; Figure 3F showed representative FCM histograms for the fluorescent intensity of DiO-labeled exosome in the RAW264.7 cells. Consistent with the *in vitro* fluorescent imaging, the quantificational data of the MFI revealed a significantly lower uptake efficiency of Exo^{CD47} compared to Exo by RAW264.7 cells. Additionally, FCM measurements confirmed that the proportion of DiO^+ RAW264.7 cells in the Exo^{CD47} treatment group was significantly lower than that observed in the Exo treatment group.

To further validate the efficacy of CD47 engineering, we extended our investigations to an *in vivo* setting. DiO-labeled Exo or Exo^{CD47} was administered intravenously into mice.

(E) Representative histograms indicating mean fluorescence intensity (MFI) of DiO-labeled Exo and RLTR-Exo in LSEC. Quantitative data of the MFI of DiO-labeled Exo and RLTR-Exo in LSEC. FCM analysis of $FITC^+$ LSEC ratio after intravenous administration of DiO-labeled Exo and RLTR-Exo. Exo: $n = 4$, RLTR-Exo: $n = 5$.

(F) Schematic diagram of single and sequential strategies.

(G) Immunofluorescence of liver frozen sections collected from mice with different injection strategies showing the cellular uptake and internalization of exosomes by LSEC. Quantitative data of the internalized DiO-labeled exosomes by LSECs with different injection strategies. Red: LYVE1. Green: DiO-labeled Exo and RLTR-Exo. Blue: DAPI-labeled nuclei. Exo: $n = 5$, RLTR-Exo: $n = 6$, Exo + Exo: $n = 3$, Exo + RLTR-Exo: $n = 3$. Scale bar: 50 μm.

Data are represented as mean ± SD (error bars) from biological replicates. Statistical analyses, n.s., not significant, $^*p < 0.05$, $^{**}p < 0.01$, $^{***}p < 0.001$, $^{****}p < 0.0001$. Statistical significance was determined by unpaired Student's t test or one-way ANOVA where appropriate. See also Figure S1.

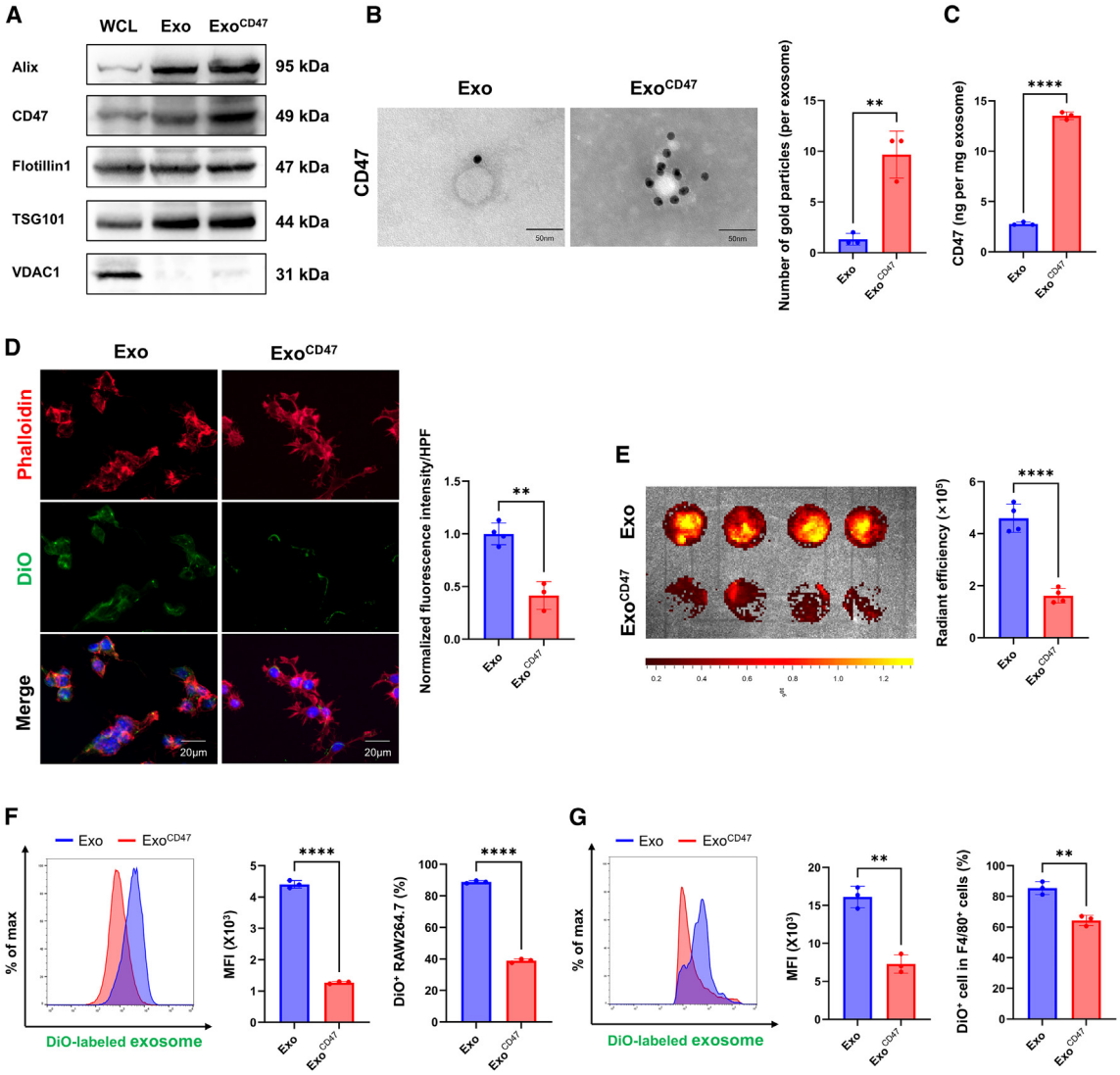

Figure 3. CD47 engineering exosome escapes the phagocytosis by macrophages

(A) WB analysis for Alix, Flotillin1, TSG101, VDAC1, and CD47 of bEnd.3 whole-cell lysate (WCL), Exo, and Exo^{CD47}.

(B) TEM imaging and gold particles quantification of immune-gold-labeled Exo and Exo^{CD47}. Gold particles are depicted as black dots. $n = 3$. Scale bar, 50 nm.

(C) ELISA of CD47 on the surface of Exo and Exo^{CD47}. $n = 3$.

(D) CLSM images of internalization of Exo and Exo^{CD47} by RAW264.7. Red: TRITC-phalloidin-labeled F-actin. Green: DiO-labeled Exo and RLTR-Exo. Blue: DAPI-labeled nuclei. Exo: $n = 4$, Exo^{CD47}: $n = 3$. Scale bar: 20 μm.

(E) *Ex vivo* fluorescence image showing the retention of DiI-labeled Exo (up) and Exo^{CD47} (down) in RAW264.7 at 1 h after incubation. $n = 4$.

(F) Representative histograms indicating mean fluorescence intensity (MFI) of DiO-labeled Exo and Exo^{CD47} in RAW264.7. Quantitative data of the MFI of DiO-labeled Exo and Exo^{CD47} in RAW264.7. FCM analysis of FITC$^+$ RAW264.7 ratio after incubation with DiO-labeled Exo and Exo^{CD47}. $n = 3$.

(G) Representative histograms indicating mean fluorescence intensity (MFI) of DiO-labeled Exo and Exo^{CD47} in KCs. FCM analysis of FITC$^+$ KC ratio after intravenous administration of DiO-labeled Exo and Exo^{CD47}. $n = 3$.

Data are represented as mean ± SD (error bars) from biological replicates. Statistical analyses, n.s., not significant, $^{**}p < 0.01$, $^{****}p < 0.0001$. Statistical significance was determined by unpaired Student's t test. See also Figure S2.

Primary mouse liver NPCs were isolated after 12 h, and FCM was employed to examine the distribution of exosomes within KCs. Figure 3G presented the representative FCM histograms illustrating the fluorescence intensity of DiO-labeled exosomes in KCs. The quantitative data on MFI indicated a significant decrease in the uptake efficiency of Exo^{CD47} by KCs compared to Exo. Moreover, FCM analyses confirmed that the ratio of DiO$^+$ KCs in the Exo^{CD47}-treated group was significantly lower compared to the Exo-treated group.

These results demonstrated that the CD47 engineering of exosome effectively inhibits macrophage phagocytosis both *in vitro* and *in vivo*.

Encapsulation of functional Wnt2 mRNA into engineered exosome

CD47^{OE}-bEnd.3 was transfected with a lentiviral vector encoding Wnt2, resulting in the establishment of the CD47^{OE}& Wnt2^{OE}-bEnd.3 cell line with a marked increase in Wnt2 expression. Exosome (Wnt2@Exo^{CD47}) was isolated from the CD47^{OE}&Wnt2^{OE}-bEnd.3 cells via ultracentrifugation, and quantitative reverse-transcription PCR (RT-qPCR) analysis indicated a substantial increase in the expression of Wnt2 mRNA in Wnt2@Exo^{CD47}, approximately 100-fold higher than control exosome (Figure 4A).

To evaluate the therapeutic potential of Wnt2 mRNA-containing exosome *in vitro*, we treated 293T, human umbilical vein endothelial cell (HUVEC), and especially primary LSEC with Exo or Wnt2@Exo^{CD47} for subsequent analysis. At first, we incubated these cells with DiO-labeled exosomes to determine their internalization. DiO signals were detected via CLSM after incubation for 4 h, and images confirmed the uptake of exosomes by the 293T, HUVEC, and LSEC (Figure 4B). Subsequently, the Wnt2 concentration in culture supernatants of these cells was detected by ELISA after incubation for 48 h. As shown in Figure 4C, incubation with Wnt2@Exo^{CD47} resulted in an elevation of Wnt2 levels in the supernatants compared to those in Exo.

Primary LSECs were isolated from 8-week-old healthy male mice and incubated with Wnt2@Exo^{CD47}, and successful mRNA delivery into LSEC was further confirmed by elevated Wnt2 mRNA expression measured via RT-qPCR in primary LSECs treated with Wnt2@Exo^{CD47} for 48 h (Figure 4D). Subsequently, we isolated primary hepatocyte from wild-type C57 mice and cultured in a 12-well plate, to which we added conditioned medium (CM) from LSEC pre-incubated with Exo or Wnt2@Exo^{CD47}. After 24 h, the treatment with Wnt2@Exo^{CD47}-CM significantly induced the upregulation of downstream target genes of the Wnt signaling pathway in the primary hepatocytes (Figure 4E).

In summary, these findings demonstrate that functional Wnt2 mRNA can be stably encapsulated within exosome and that this Wnt2 mRNA delivery system can significantly increase Wnt2 protein expression *in vitro*. Exosomes derived from CD47^{OE}&Wnt2^{OE}-bEnd.3 were then surface modified with RLTR peptides, which enhanced the secretion of Wnt2 from LSEC into the sinusoidal niche, activating the Wnt/β-catenin signaling pathway in hepatocytes. This approach holds promise as a therapeutic strategy for the treatment of acute liver injury.

The engineered exosome treatment ameliorates acute liver injury

To further explore the therapeutic effects of the engineered exosomes, an acute liver injury model was induced by dimethyl nitrosamine (DMN) or acetaminophen (APAP). Firstly, to test the LSEC-targeting efficiency of RLTR-Wnt2@Exo^{CD47} *in vivo*, DMN/APAP acute liver injury mice were infused with Exo, DiI-labeled Exo, or DiI-labeled RLTR-Wnt2@Exo^{CD47} for analysis. Figure S3A showed *ex vivo* fluorescence imaging of main organs from mice 12 h post-injection, revealing higher liver accumulation of RLTR-Wnt2@Exo^{CD47} compared to Exo in both injury models. Immunofluorescence staining of organ sections also confirmed the liver enrichment of DiI-labeled RLTR-Wnt2@Exo^{CD47} post-injection (Figure S3B). Moreover, CLSM images of liver sections showed the presence of DiI-labeled RLTR-Wnt2@Exo^{CD47} in LYVE1^{+} LSEC 12 h after injection in both of DMN and APAP models (Figure S3C). The co-localization of DiI-labeled RLTR-Wnt2@Exo^{CD47} with LSEC was indicated by the white arrows. These results indicated that RLTR and CD47 surface modification effectively enhanced exosome targeting to LSEC, and the engineered exosome retained this property in acute liver injury mice induced by DMN/APAP.

Next, we examined the therapeutic efficacy of RLTR-Wnt2@Exo^{CD47} in APAP/DMN-induced liver injury mice models. Mice received DMN or APAP intraperitoneally and were simultaneously infused with single dose of PBS, control Exo, or RLTR-Wnt2@Exo^{CD47} (200 μg per mouse) through the tail vein. For DMN-induced liver injury, the samples were harvested 48 h after DMN administration (Figure 5A). The overall appearance of the mice livers indicated that the RLTR-Wnt2@Exo^{CD47} treatment group showed significant improvement in hepatic congestion compared to the PBS/Exo treatment group (Figure 5B). Serum biochemical tests revealed that, compared to the PBS/Exo treatment group, RLTR-Wnt2@Exo^{CD47} treatment significantly decreased the levels of alanine aminotransferase (ALT), aspartate aminotransferase (AST), and total bilirubin (TBIL) in serum and increased the levels of albumin (ALB) (Figure 5C). Despite the levels of ALT, AST, and TBIL post-treatment with RLTR-Wnt2@Exo^{CD47} being still above normal range, they indicated partial liver function improvement. Moreover, the engineered exosome mitigated liver injury by promoting hepatocyte proliferation as indicated by ki67 staining (Figures 5E and 5H), with decreased liver necrotic areas in the RLTR-Wnt2@Exo^{CD47} group as evidenced by H&E staining (Figures 5G and 5I). TUNEL staining analysis demonstrated a lower incidence of hepatocellular death in the RLTR-Wnt2@Exo^{CD47} group following DMN administration compared to the PBS/Exo group (Figures S4A and S4D). Inflammatory cells, such as macrophages and neutrophils, were recruited and infiltrated the necrotic areas. The results of immunofluorescence staining in Figures S4B and S4E showed that, compared to the PBS/Exo group, the infiltration of LY6G-positive neutrophils in the necrotic areas was significantly reduced in the RLTR-Wnt2@Exo^{CD47} treatment group. In addition, we performed F4/80 and CLEC4F double staining to distinguish KCs and infiltrated inflammatory macrophages. Immunofluorescence staining revealed that macrophages were extensively infiltrated in the PBS/Exo group, while the distribution of macrophages in the RLTR-Wnt2@Exo^{CD47} treatment group was significantly limited (Figures S4C and S4F).

To evaluate the therapeutic efficacy of engineered exosomes in APAP-induced liver injury, we systematically analyzed three parameters at multiple post-injury time points: (1) liver-to-body weight ratio (Figure S5A); (2) serum levels of ALT, AST, TBIL, and ALB (Figure S5B); and (3) hepatic histomorphology (Figures S5C and S5D). Based on these temporal analyses, 36 h post-APAP administration was selected as the optimal therapeutic window for exosome intervention prior to terminal analysis (Figure 5A). Consistent with our hypothesis, RLTR-Wnt2@Exo^{CD47} demonstrated significant hepatoprotective effects in the APAP-induced injury model. Macroscopic

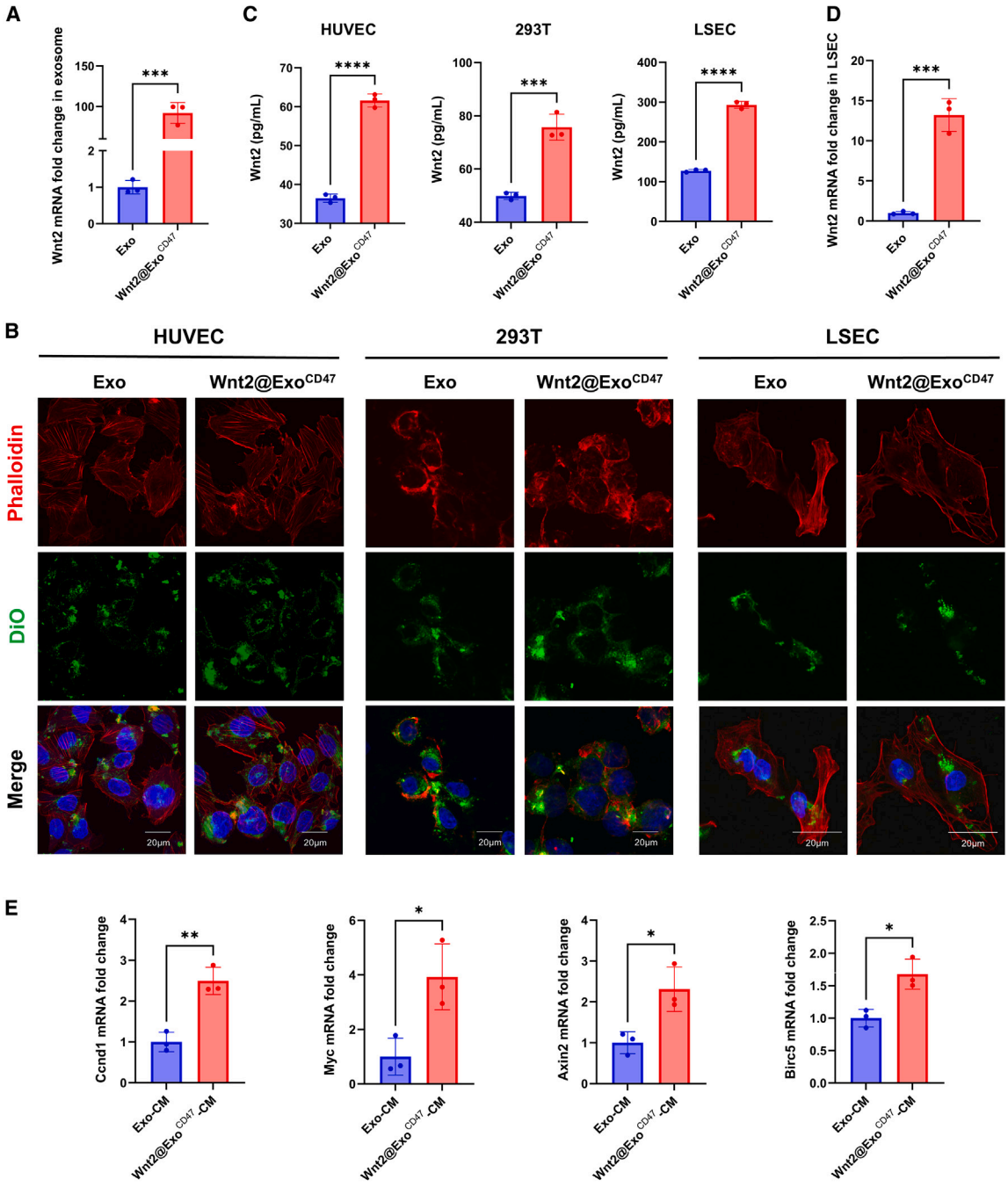

Figure 4. Efficacy of Wnt2 mRNA-loaded exosome *in vitro*

(A) Wnt2 mRNA expression in Exo and Wnt2@Exo^{CD47} detected by RT-qPCR. $n = 3$.

(B) CLSM images showing the internalization of DiO-labeled Exo and Wnt2@Exo^{CD47} by HUVEC (left), 293T (meddle), and primary LSEC (right). Red: TRITC-phalloidin-labeled F-actin. Green: DiO-labeled Exo and Wnt2@Exo^{CD47}. Blue: DAPI-labeled nuclei. Scale bar: 20 μm

(C) ELISA analysis of Wnt2 concentration in culture supernatant of HUVEC (left), 293T (meddle), and primary LSEC (right) at 48 h after incubation with Exo and Wnt2@Exo^{CD47}. $n = 3$.

(D) RT-qPCR shows higher Wnt2 mRNA transcript levels after *in vitro* delivery of Wnt2 mRNA from Wnt2@Exo^{CD47} (Exo vs. Wnt2@Exo^{CD47}) in 48 h. $n = 3$.

(E) Following incubation with conditioned medium for 24 h, RT-qPCR was employed to analyze the changes in downstream target genes of the Wnt pathway in the primary hepatocytes. $n = 3$.

Data are represented as mean ± SD (error bars) from biological replicates. Statistical analyses, n.s., not significant, $^{*}p < 0.05$, $^{**}p < 0.01$, $^{***}p < 0.001$, $^{****}p < 0.0001$. Statistical significance was determined by unpaired Student's t test.

CellPress
OPEN ACCESS

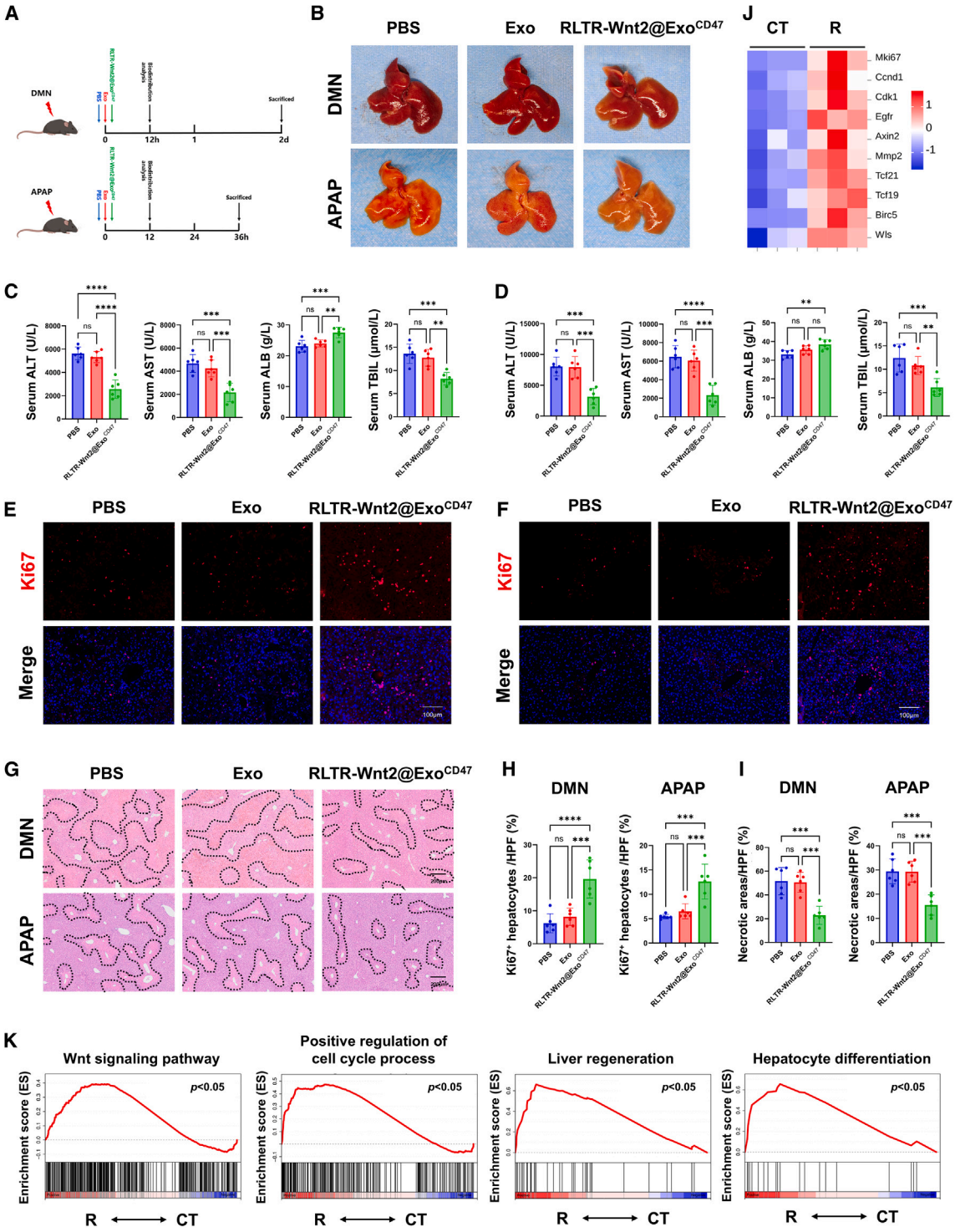

Figure 5. The engineered exosome treatment alleviates DMN/APAP-induced acute liver injury

(A) Schematic illustration of the experimental procedure.

(B) The overall appearance of the livers in DMN (up)- and APAP (down)-induced acute liver injury mice after tail vein administration of PBS, Exo, or RLTR-Wnt2@Exo^{CD47}.

(C) Serum ALT, AST, ALB, and TBIL of mice with DMN-induced liver injury at 48 h after PBS, Exo, or RLTR-Wnt2@Exo^{CD47} administration. $n = 6$. ALB, albumin; ALT, alanine aminotransferase; AST, aspartate aminotransferase; TBIL, total bilirubin.

(legend continued on next page)

evaluation revealed restored hepatic coloration and improved gross morphology in the RLTR-Wnt2@Exo^{CD47}-treated group compared to controls (Figure 5B). Biochemical analysis further confirmed enhanced liver function, with marked reductions in serum ALT, AST, and TBIL, alongside a positive trend in ALB levels (Figure 5D). We next evaluated hepatocyte proliferation, which counteracts the injury to drive liver repair. Ki67-positive hepatocytes in the RLTR-Wnt2@Exo^{CD47} group were significantly more than those in the PBS/Exo group (Figures 5F and 5H), and RLTR-Wnt2@Exo^{CD47}-treated mice exhibited a significantly reduced necrotic areas as shown by H&E staining (Figures 5G and 5I). TUNEL staining showed that treatment with RLTR-Wnt2@Exo^{CD47} significantly reduced hepatocellular death (Figures S4A and S4D). Notably, immunofluorescence analysis demonstrated more localized immune responses in RLTR-Wnt2@Exo^{CD47}-treated livers, characterized by less infiltration of neutrophils (Ly6G^{+}) and inflammatory macrophages (CLEC4F^{-}/F4/80^{+}) within peri-necrotic regions (Figures S4B, S4C, S4E, and S4F).

APAP is a common cause of DILI in clinical settings. To comprehensively analyze the gene expression profiles in the liver of APAP model, RNA sequencing (RNA-seq) was performed on liver tissues from different treatment groups. This approach enabled the quantification of global gene expression changes and the identification of gene transcription alterations associated with therapeutic interventions (Table S2). We assessed the related gene expressions in Wnt- and liver regeneration-related signaling pathways. Notably, genes pivotal for hepatocyte proliferation, such as ki67 and Cdk1, were upregulated in the RLTR-Wnt2@Exo^{CD47} group. Similarly, key downstream targets of Wnt signaling pathway, such as Ccnd1, Axin2, and Mmp2, were also upregulated compared to the control group (Figure 5J). Gene set enrichment analysis (GSEA) indicated that the gene signatures associated with the Wnt signaling pathway, positive regulation of the cell cycle, liver regeneration, and hepatocyte differentiation were significantly upregulated, as shown in Figure 5K.

Overall, these results suggested that RLTR-Wnt2@Exo^{CD47} treatment ameliorated acute liver injury by promoting proliferation of hepatocytes in DMN/APAP mice.

Preliminary safety evaluation of the engineered exosome

The biosafety of RLTR-Wnt2@Exo^{CD47} was also briefly evaluated both *in vitro* and *in vivo*. Cytotoxicity of RLTR-Wnt2@Exo^{CD47} was assessed using bEnd.3 cells *in vitro*. Cell viability of bEnd.3 was analyzed by cell counting kit-8 (CCK8) assay after incubation with different concentrations of Exo or RLTR-Wnt2@Exo^{CD47} for 12, 24, and 48 h. The CCK8 results indicated that RLTR-Wnt2@Exo^{CD47} did not exert cytotoxic effects on bEnd.3 cells at concentrations up to 100 μg/mL across all time points examined (Figure 6A). Furthermore, RLTR-Wnt2@Exo^{CD47} treatment enhanced cell proliferation in a time-dependent manner compared to the Exo treatment group.

For *in vivo* evaluation, healthy mice were administered via the tail vein with PBS or approximately 200 μg (protein equivalent) of Exo or RLTR-Wnt2@Exo^{CD47} suspended in 200 μL of PBS. After 48 h, blood and main organs were collected from these mice for detailed examination (Figure 6B). Liver function indicators ALT, AST, ALB, and TBIL (Figure 6C); kidney function indicators blood urea nitrogen (BUN) and creatine (CREA) (Figure 6D); and heart function indicators lactate dehydrogenase (LDH) and lactate dehydrogenase 1 (LDH1) (Figure 6E) were all measured. These indicators except for kidney function indicators were not significantly shifted after RLTR-Wnt2@Exo^{CD47} treatment, suggesting that the engineered exosome was non-toxic. Especially, as shown in Figure 6D, the level of BUN and CREA in the RLTR-Wnt2@Exo^{CD47} group was not significantly different from that in the PBS group, and the level of BUN was significantly lower in the RLTR-Wnt2@Exo^{CD47} group than in the Exo group, indicating reduced nephrotoxicity.

Finally, heart, liver, spleen, lung, and kidney samples were sectioned and H&E stained (Figure 6F). The images showed no signs of necrosis or inflammation in these organs induced by RLTR-Wnt2@Exo^{CD47}, indicating its biocompatibility and the absence of acute damage to major organs.

DISCUSSION

Despite their relatively small proportion within the hepatic microenvironment, extensive research has demonstrated the key role of LSECs in liver regeneration.[20,21] This established biological significance positions LSEC as a promising therapeutic target for acute liver injury treatment.[22] The Wnt/β-catenin signaling pathway operates as a master regulatory axis governing both hepatic metabolic zonation maintenance and injury-induced hepatocyte proliferation.[23–26] Hu et al. revealed conserved expression patterns of Wnt2 and Wnt9b in liver endothelial cells, genetic ablation of them in LSEC led to abrogation pericentral (zone 3) gene expression programs, induced ectopic periportal (zone 1)

(D) Serum ALT, AST, ALB, and TBIL of mice with APAP-induced liver injury at 48 h after PBS, Exo, or RLTR-Wnt2@Exo^{CD47} administration. $n = 6$. ALB, albumin; ALT, alanine aminotransferase; AST, aspartate aminotransferase; TBIL, total bilirubin.

(E and F) Ki67 immunofluorescence staining of DMN (E)- and APAP (F)-injured liver after PBS, Exo, or RLTR-Wnt2@Exo^{CD47} administration. Red: ki67. Blue: nuclei. Scale bar: 100 μm.

(G) H&E staining of liver collected from DMN (up) and APAP (down) mice after treated with PBS, Exo, or RLTR-Wnt2@Exo^{CD47}. Scale bar: 200 μm.

(H) Quantitative analysis of the Ki67^{+} hepatocytes ratio. $n = 6$.

(I) Quantitative analysis of the necrotic areas. $n = 6$.

(J) The heatmap based on the differently expressed genes between livers from control and RLTR-Wnt2@Exo^{CD47} group. Data were obtained from biological replicates. CT: control group, R: RLTR-Wnt2@Exo^{CD47} group.

(K) GSEA revealing the enrichment of differently expressed genes in the Wnt, positive regulation of cell-cycle process, liver regeneration, and hepatocyte differentiation signaling pathways. $n = 3$. CT, control group; R, RLTR-Wnt2@Exo^{CD47} group.

Data are represented as mean ± SD (error bars) from biological replicates. Statistical analyses, n.s., not significant, $^{**}p < 0.01$, $^{***}p < 0.001$, $^{****}p < 0.0001$. Statistical significance was determined by one-way ANOVA. See also Figures S3–S6.

CellPress
OPEN ACCESS

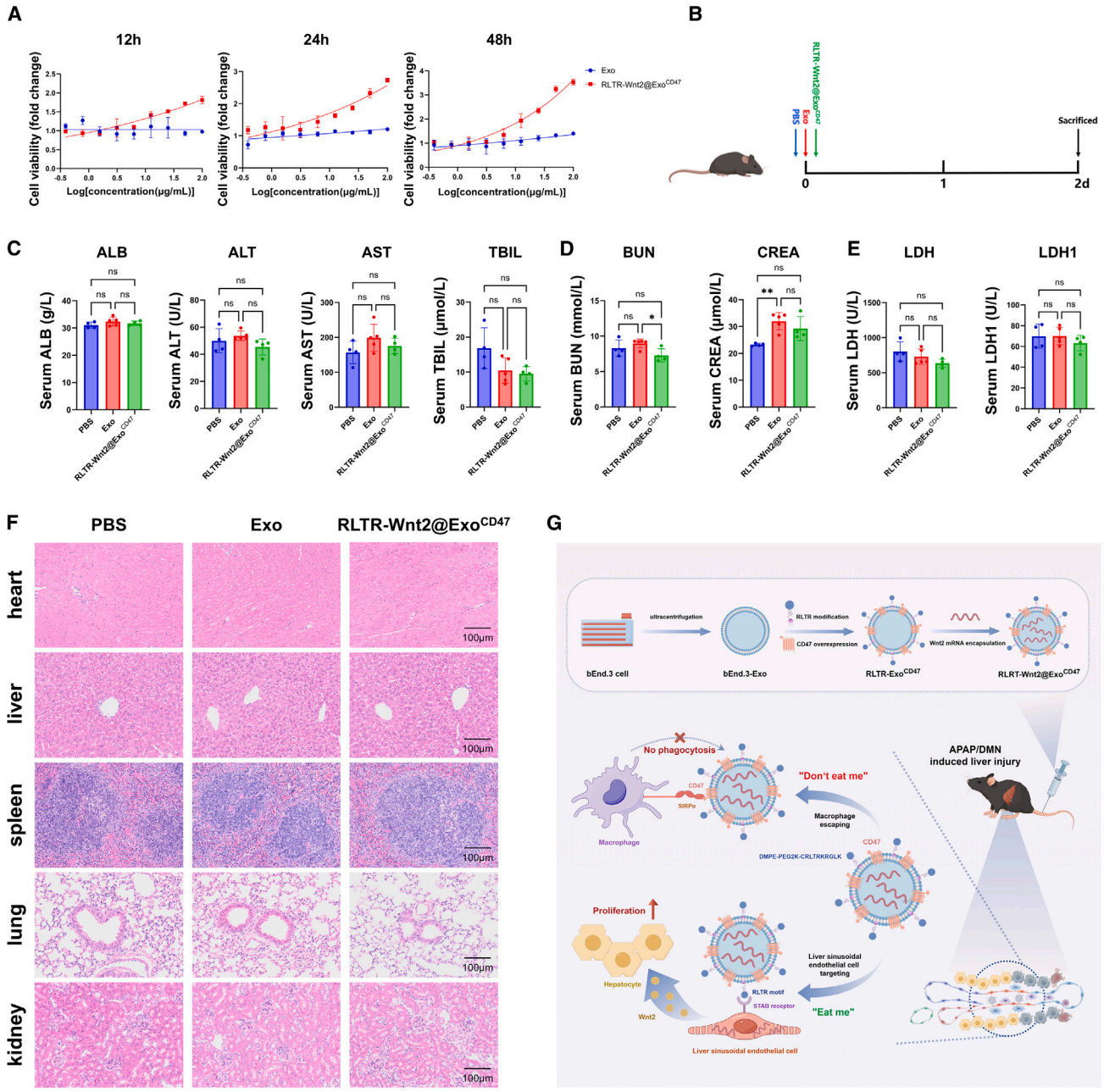

Figure 6. Safety evaluation of the engineered exosome *in vitro* and *in vivo*

(A) Cell viability of bEnd.3 was analyzed by CCK8 assay after incubation with different concentrations of Exo or RLTR-Wnt2@Exo^{CD47} at 12, 24, and 48 h. $n = 3$.

(B) Scheme showing the treatment timeline of PBS, Exo, and RLTR-Wnt2@Exo^{CD47}.

(C–E) Quantitative analysis of serological detection indicators about liver function (C), renal function (D), and myocardial enzymes (E) in serum of mice with different treatment. PBS: $n = 4$, Exo: $n = 5$, RLTR-Wnt2@Exo^{CD47}: $n = 4$. ALB, albumin; ALT, alanine aminotransferase; AST, aspartate aminotransferase; TBIL, total bilirubin; BUN, blood urea nitrogen; CREA, creatine; LDH, lactate dehydrogenase; LDH1, lactate dehydrogenase 1.

(F) H&E-stained images of the major organs (heart, liver, spleen, lung, and kidney) collected from mice in different treatment groups after sacrifice. Scale bar: 100 μm.

(G) Schematic showed the working model of this study. Exosomes are isolated from bEnd.3 culture medium and engineered with a dual-targeting "eat me/don't eat me" strategy, enabling them to evade macrophage phagocytosis while specifically targeting LSEC. Engineered exosomes deliver Wnt2 mRNA to LSEC, enhancing the release of Wnt2 into the sinusoidal niche. This activates the Wnt/β-catenin signaling pathway in hepatocytes, driving liver regeneration following acute liver injury.

Data are represented as mean ± SD (error bars) from biological replicates. Statistical analyses, n.s., not significant, $^{*}p < 0.05$, $^{**}p < 0.01$. Statistical significance was determined by one-way ANOVA.

marker expression in central regions, and blunted liver regeneration.[6] Zhao et al. demonstrated the importance of the Wnt/β-catenin signaling pathway in restoring tissue integrity following acute liver toxicity and established a role of endothelial cells as an important Wnt-producing regulator of liver tissue repair following localized liver injury.[5] These collective findings established endothelial-secreted Wnt ligands, particularly Wnt2, as fundamental mediators of post-injury hepatic restitution. Therapeutic potentiation of LSEC-derived Wnt2 secretion following acute hepatic damage may therefore represent a viable strategy to enhance parenchymal regeneration and accelerate functional recovery.

LSEC constitutes critical mediators in hepatic pathophysiology, participating in both disease initiation and progression across multiple liver disorders.[27,28] There is a range of endocytic receptors expressed on the surface of LSEC; these receptors enable precision drug delivery through ligand-receptor recognition mechanisms.[22] Mannan was selected as a ligand to target the mannose receptor, while an ApoB peptide, RLTRKRGLK, was utilized as a ligand for Stabilin receptors. Stabilin receptors are exclusively expressed on LSEC, whereas the mannose receptor is also present in low abundance on the surface of KC.[29] Structural analysis reveals that both RLTRKRGLK and reverse-sequence KLGRKRTLR (KLGR) accumulate extensively in LSEC. Both peptides contain the same RXR or RXXR motif, which may account for their significant enrichment in LSEC.[13] This motif-directed targeting paradigm has been successfully translated into therapeutic platforms. Liu et al. accurately delivered mouse ovalbumin allergen to LSEC through RXXR peptide-coated biodegradable polymer poly (lactic-co-glycolic acid) nanocarriers, inducing LSEC to produce high levels of transforming growth factor β, interleukin (IL)-4, and IL-10. Pretreatment in mice led to a significant improvement of airway inflammation in murine asthma models.[30] These findings establish RLTR or KLGR peptides as engineering ligands for LSEC-targeted drug delivery systems.

The lipid bilayer membrane structure of exosome facilitates the stable encapsulation and transmission of biological cargo from donor cells, mediating intercellular communication. Consequently, these natural nanocarriers hold promise for drug delivery. Compared to synthetic drug carriers, exosomes exhibit excellent biocompatibility and reduced toxicity.[31] Moreover, exosomes are highly engineerable, and, by surface engineering, they can be employed to achieve targeted delivery to specific tissues or even individual cells.[32] The hydrophobic insertion method has been utilized for exosome modification,[12,33] leveraging the hydrophobic interaction between the exosome membrane and lipid conjugates, allowing for the engineering of the membrane surface while preserving the biological functionality of the exosomes.[11] In this study, we synthesized the amphiphilic compound DMPE-PEG2000-CRLTRKRGLK, where hydrophobic moiety efficiently inserts into the lipid bilayer membrane of exosome, thereby modifying the surface with the LSEC-targeting peptides RXXR motif.

The liver harbors the largest population of tissue-resident macrophages.[34] KCs account for approximately 90% of all tissue macrophages within the body, and they are responsible for the capture and clearance of foreign materials,[35] leading to the "off-target" drug effects, impaired therapeutic efficacy, and even unexpected adverse reactions. Therefore, understanding and controlling phagocytosis by macrophages are extremely critical for developing potential nanotherapeutics, but this remains a significant challenge. In recent years, various strategies have been designed to reduce the non-specific accumulation of nanoparticles in macrophages. Some studies have modified the nanocarriers with CD47 or its derived peptides,[14,15,36] which significantly prevents phagocytosis by macrophages, thereby enabling precise delivery of the drug.

mRNA-based therapeutics offer transformative potential across vaccine development, protein replacement therapies, and the treatment of genetic disorders.[37] However, application of mRNA is still limited by the need for improved delivery systems. Methods and vehicles for intracellular delivery remain the major barrier to the broad application of mRNA therapeutics. With some exceptions, the intracellular delivery of mRNA is generally more challenging than that of small oligonucleotides, and it requires encapsulation into a delivery nanoparticle, in part due to the significantly larger size of mRNA molecules (300–5,000 kDa) as compared to other types of RNAs (small interfering RNAs, ∼14 kDa; antisense oligonucleotides, 4–10 kDa). In this study, we engineered Wnt2 mRNA-enriched exosomes by transfecting exosome-source cells bEnd.3 with the mouse Wnt2 gene-overexpressing lentivirus. The results of the RT-qPCR experiment revealed that the exosome from lentivirus-transfected cells had approximately 100-fold higher Wnt2 mRNA expression than control exosome. Future experiments should focus on optimizing the encapsulation strategy for Wnt2 mRNA to enhance therapeutic outcomes.

In this study, we administered engineered exosome immediately following the intraperitoneal injection of DMN/APAP in mice and observed positive therapeutic effects. However, to better simulate clinical scenarios where patients typically present with delayed hepatotoxicity symptoms rather than at initial toxicant exposure, we implemented a modified treatment protocol. Specifically, engineered exosomes were administered at pathologically relevant time points corresponding to peak liver injury profiles (2 days post-DMN and 36 h post-APAP injection, as established in previous studies). Subsequent analyses were conducted 48 h post-treatment. Compared to the PBS/Exo treatment, the administration of RLTR-Wnt2@Exo^{CD47} did not significantly alter the overall appearance of the livers in DMN/APAP model mice (Figure S6A). Blood biochemical tests (Figure S6B) suggested a slight improvement in liver function, particularly a significant reduction in serum ALT levels, in the APAP model. Further analysis of H&E-stained liver sections across various treatment groups within the DMN/APAP model showed a slight reduction of liver necrotic areas in the RLTR-Wnt2@Exo^{CD47}-treated group, though not statistically significant (Figures S6C and S6D). The observed therapeutic limitations may be due to severe congestion in the liver sinusoids after injury, which could impede the intravenously administered engineered exosomes from effectively reaching LSEC for drug delivery.

In conclusion, we have proposed and successfully constructed a dual-targeting strategy of "eat me/don't eat me"

based on exosome. Exo^{CD47} was engineered by overexpressing the mouse CD47 gene in bEnd.3, which has been proven to significantly inhibit the phagocytosis by macrophages. Meanwhile, the exosome membrane was functionally modified with DMPE-PEG2000-CRLTRKRGLK, leveraging RXR/RXXR motifs-mediated receptor binding to enhance cellular internalization by LSEC. Furthermore, therapeutic nucleic acid drugs (Wnt2 mRNA) were loaded into the exosomes. Finally, the resulting engineered exosome maintained superior LSEC-targeting specificity and displayed potent therapeutic efficacy in DMN/APAP-induced liver injury mice (Figure 6G).

Limitations of the study

Although administration of engineered exosome has yielded the anticipated outcomes in DILI mice, there is potential for further improvement in our study. The liver has remarkable regenerative abilities and, in response to acute injury, swiftly initiates intrinsic repair pathways to promote the regeneration of damaged liver tissue and restore hepatic function. The DILI mouse model employed in this study is of moderate severity, with the liver retaining strong regenerative powers. The engineering exosome we developed is nothing more than accelerating the process of liver regeneration. To comprehensively evaluate the therapeutic potential of our engineered exosomes, it is necessary to assess their efficacy in a broader spectrum of animal models, including those exposed to lethal levels of APAP and extensive hepatectomy (such as 90% hepatectomy).

RESOURCE AVAILABILITY

Lead contact

Further information and requests for resources and reagents should be directed to and will be fulfilled by the lead contact, Lin Wang (fierywang@163.com).

Materials availability

All unique/stable reagents generated in this study are accessible from the lead contact with a completed Materials Transfer Agreement.

Data and code availability

- The raw reads of our transcriptome data have been deposited into the NCBI Sequence Read Archive (SRA, https://www.ncbi.nlm.nih.gov/sra/) under the accession number PRJNA1213977.
- This paper does not generate original code. All data associated with this study are presented in the paper or supplemental information.
- Any additional information required to reanalyze the data reported in this paper is available from the lead contact upon request.

ACKNOWLEDGMENTS

This work was supported by grants from the National Natural Science Foundation of China (82325007 and 92468202) and the National Key Research and Development Program of China (2021YFA1100502). The graphical abstract (export ID is TOTOId4747) and schematic diagrams (export ID is YAITT4d4dd) were created with Figdraw.

AUTHOR CONTRIBUTIONS

Conceptualization, W.D. and H.Q.; methodology, W.D. and H.Q.; investigation, C.C., Y. Liu, M.X., J.L., P.S., Z.F., Z.Y., H.X., and Y. Ling; writing – original draft, W.D. and H.Q.; writing – review and editing, W.D., J.D., and F.H.; funding acquisition, L.W.; resources, J.D. and F.H.; supervision, L.W.

DECLARATION OF INTERESTS

The authors declare no competing interests.

STAR★METHODS

Detailed methods are provided in the online version of this paper and include the following:

- KEY RESOURCES TABLE
- EXPERIMENTAL MODEL AND STUDY PARTICIPANT DETAILS
  - Experimental mouse models and exosomes injection
  - Cell culture and transfection
- METHOD DETAILS
  - Exosome isolation and labeling
  - Synthesis of DMPE-PEG2000-CRLTRKRGLK
  - Preparation and characterization of RLTR-Exo
  - Isolation of primary hepatic cells
  - Western blotting
  - *In vivo* biodistribution study
  - *In vitro* cellular uptake study
  - Evaluation of liver injury
  - Cytotoxicity evaluation
  - *In vivo* toxicity study
- QUANTIFICATION AND STATISTICAL ANALYSIS

SUPPLEMENTAL INFORMATION

Supplemental information can be found online at https://doi.org/10.1016/j.xcrm.2025.102033.

Received: July 4, 2024
Revised: December 9, 2024
Accepted: February 24, 2025
Published: March 21, 2025

REFERENCES

1. Andrade, R.J., Chalasani, N., Björnsson, E.S., Suzuki, A., Kullak-Ublick, G.A., Watkins, P.B., Devarbhavi, H., Merz, M., Lucena, M.I., Kaplowitz, N., and Aithal, G.P. (2019). Drug-induced liver injury. Nat. Rev. Dis. Primers *5*, 58.
2. Yan, M., Huo, Y., Yin, S., and Hu, H. (2018). Mechanisms of acetaminophen-induced liver injury and its implications for therapeutic interventions. Redox Biol. *17*, 274–283.
3. Tujios, S.R., and Lee, W.M. (2018). Acute liver failure induced by idiosyncratic reaction to drugs: Challenges in diagnosis and therapy. Liver Int. *38*, 6–14.
4. Gracia-Sancho, J., Caparrós, E., Fernández-Iglesias, A., and Francés, R. (2021). Role of liver sinusoidal endothelial cells in liver diseases. Nat. Rev. Gastroenterol. Hepatol. *18*, 411–431.
5. Zhao, L., Jin, Y., Donahue, K., Tsui, M., Fish, M., Logan, C.Y., Wang, B., and Nusse, R. (2019). Tissue Repair in the Mouse Liver Following Acute Carbon Tetrachloride Depends on Injury-Induced Wnt/β-Catenin Signaling. Hepatology *69*, 2623–2635.
6. Hu, S., Liu, S., Bian, Y., Poddar, M., Singh, S., Cao, C., McGaughey, J., Bell, A., Blazer, L.L., Adams, J.J., et al. (2022). Single-cell spatial transcriptomics reveals a dynamic control of metabolic zonation and liver regeneration by endothelial cell Wnt2 and Wnt9b. Cell Rep. Med. *3*, 100754.
7. Ma, R., Martínez-Ramírez, A.S., Borders, T.L., Gao, F., and Sosa-Pineda, B. (2020). Metabolic and non-metabolic liver zonation is established non-synchronously and requires sinusoidal Wnts. Elife *9*, e46206.
8. Moon, R.T., Kohn, A.D., De Ferrari, G.V., and Kaykas, A. (2004). WNT and beta-catenin signalling: diseases and therapies. Nat. Rev. Genet. *5*, 691–701.

9. Clevers, H., and Nusse, R. (2012). Wnt/β-catenin signaling and disease. Cell *149*, 1192–1205.
10. Zhang, M., Hu, S., Liu, L., Dang, P., Liu, Y., Sun, Z., Qiao, B., and Wang, C. (2023). Engineered exosomes from different sources for cancer-targeted therapy. Signal Transduct. Targeted Ther. *8*, 124.
11. Liang, Y., Duan, L., Lu, J., and Xia, J. (2021). Engineering exosomes for targeted drug delivery. Theranostics *11*, 3183–3195.
12. Wu, Q., Fu, X., Li, X., Li, J., Han, W., and Wang, Y. (2023). Modification of adipose mesenchymal stem cells-derived small extracellular vesicles with fibrin-targeting peptide CREKA for enhanced bone repair. Bioact. Mater. *20*, 208–220.
13. Akhter, A., Hayashi, Y., Sakurai, Y., Ohga, N., Hida, K., and Harashima, H. (2013). A liposomal delivery system that targets liver endothelial cells based on a new peptide motif present in the ApoB-100 sequence. Int. J. Pharm. *456*, 195–201.
14. Belhadj, Z., He, B., Deng, H., Song, S., Zhang, H., Wang, X., Dai, W., and Zhang, Q. (2020). A combined "eat me/don't eat me" strategy based on extracellular vesicles for anticancer nanomedicine. J. Extracell. Vesicles *9*, 1806444.
15. Rodriguez, P.L., Harada, T., Christian, D.A., Pantano, D.A., Tsai, R.K., and Discher, D.E. (2013). Minimal "Self" peptides that inhibit phagocytic clearance and enhance delivery of nanoparticles. Science *339*, 971–975.
16. Osorio, J.C., Smith, P., Knorr, D.A., and Ravetch, J.V. (2023). The antitumor activities of anti-CD47 antibodies require Fc-FcγR interactions. Cancer. Cell. *41*, 2051–2065.e6.
17. Barclay, A.N., and Van den Berg, T.K. (2014). The interaction between signal regulatory protein alpha (SIRPα) and CD47: structure, function, and therapeutic target. Annu. Rev. Immunol. *32*, 25–50.
18. Jiang, D., Burger, C.A., Akhanov, V., Liang, J.H., Mackin, R.D., Albrecht, N.E., Andrade, P., Schafer, D.P., and Samuel, M.A. (2022). Neuronal signal-regulatory protein alpha drives microglial phagocytosis by limiting microglial interaction with CD47 in the retina. Immunity *55*, 2318–2335.e7.
19. Logtenberg, M.E.W., Scheeren, F.A., and Schumacher, T.N. (2020). The CD47-SIRPα Immune Checkpoint. Immunity *52*, 742–752.
20. McConnell, M.J., Kostallari, E., Ibrahim, S.H., and Iwakiri, Y. (2023). The evolving role of liver sinusoidal endothelial cells in liver health and disease. Hepatology *78*, 649–669.
21. Duan, J.L., Zhou, Z.Y., Ruan, B., Fang, Z.Q., Ding, J., Liu, J.J., Song, P., Xu, H., Xu, C., Yue, Z.S., et al. (2022). Notch-Regulated c-Kit-Positive Liver Sinusoidal Endothelial Cells Contribute to Liver Zonation and Regeneration. Cell. Mol. Gastroenterol. Hepatol. *13*, 1741–1756.
22. Du, W., and Wang, L. (2022). The Crosstalk Between Liver Sinusoidal Endothelial Cells and Hepatic Microenvironment in NASH Related Liver Fibrosis. Front. Immunol. *13*, 936196.
23. Zeng, G., Awan, F., Otruba, W., Muller, P., Apte, U., Tan, X., Gandhi, C., Demetris, A.J., and Monga, S.P.S. (2007). Wnt'er in liver: expression of Wnt and frizzled genes in mouse. Hepatology *45*, 195–204.
24. Zhu, S., Rao, X., Qian, Y., Chen, J., Song, R., Yan, H., Yang, X., Hu, J., Wang, X., Han, Z., et al. (2022). Liver Endothelial Heg Regulates Vascular/Biliary Network Patterning and Metabolic Zonation Via Wnt Signaling. Cell. Mol. Gastroenterol. Hepatol. *13*, 1757–1783.
25. Okabe, H., Yang, J., Sylakowski, K., Yovchev, M., Miyagawa, Y., Nagarajan, S., Chikina, M., Thompson, M., Oertel, M., Baba, H., et al. (2016). Wnt signaling regulates hepatobiliary repair following cholestatic liver injury in mice. Hepatology *64*, 1652–1666.
26. Leibing, T., Géraud, C., Augustin, I., Boutros, M., Augustin, H.G., Okun, J.G., Langhans, C.D., Zierow, J., Wohlfeil, S.A., Olsavszky, V., et al. (2018). Angiocrine Wnt signaling controls liver growth and metabolic maturation in mice. Hepatology *68*, 707–722.
27. Carambia, A., Freund, B., Schwinge, D., Bruns, O.T., Salmen, S.C., Ittrich, H., Reimer, R., Heine, M., Huber, S., Waurisch, C., et al. (2015). Nanoparticle-based autoantigen delivery to Treg-inducing liver sinusoidal endothelial cells enables control of autoimmunity in mice. J. Hepatol. *62*, 1349–1356.
28. Yu, X., Chen, L., Liu, J., Dai, B., Xu, G., Shen, G., Luo, Q., and Zhang, Z. (2019). Immune modulation of liver sinusoidal endothelial cells by melittin nanoparticles suppresses liver metastasis. Nat. Commun. *10*, 574.
29. Yu, Z., Guo, J., Liu, Y., Wang, M., Liu, Z., Gao, Y., and Huang, L. (2022). Nano delivery of simvastatin targets liver sinusoidal endothelial cells to remodel tumor microenvironment for hepatocellular carcinoma. J. Nanobiotechnol. *20*, 9.
30. Liu, Q., Wang, X., Liu, X., Kumar, S., Gochman, G., Ji, Y., Liao, Y.P., Chang, C.H., Situ, W., Lu, J., et al. (2019). Use of Polymeric Nanoparticle Platform Targeting the Liver To Induce Treg-Mediated Antigen-Specific Immune Tolerance in a Pulmonary Allergen Sensitization Model. ACS Nano *13*, 4778–4794.
31. Kalluri, R., and LeBleu, V.S. (2020). The biology, function, and biomedical applications of exosomes. Science *367*, eaau6977.
32. Li, Q., Fu, X., Kou, Y., and Han, N. (2023). Engineering strategies and optimized delivery of exosomes for theranostic application in nerve tissue. Theranostics *13*, 4266–4286.
33. Zheng, G., Ma, H.W., Xiang, G.H., He, G.L., Cai, H.C., Dai, Z.H., Chen, Y.L., Lin, Y., Xu, H.Z., Ni, W.F., et al. (2022). Bone-targeting delivery of platelet lysate exosomes ameliorates glucocorticoid-induced osteoporosis by enhancing bone-vessel coupling. J. Nanobiotechnol. *20*, 220.
34. Guilliams, M., Dutertre, C.A., Scott, C.L., McGovern, N., Sichien, D., Chakarov, S., Van Gassen, S., Chen, J., Poidinger, M., De Prijck, S., et al. (2016). Unsupervised High-Dimensional Analysis Aligns Dendritic Cells across Tissues and Species. Immunity *45*, 669–684.
35. Jenne, C.N., and Kubes, P. (2013). Immune surveillance by the liver. Nat. Immunol. *14*, 996–1006.
36. Kojima, Y., Volkmer, J.P., McKenna, K., Civelek, M., Lusis, A.J., Miller, C.L., Direnzo, D., Nanda, V., Ye, J., Connolly, A.J., et al. (2016). CD47-blocking antibodies restore phagocytosis and prevent atherosclerosis. Nature *536*, 86–90.
37. Kowalski, P.S., Rudra, A., Miao, L., and Anderson, D.G. (2019). Delivering the Messenger: Advances in Technologies for Therapeutic mRNA Delivery. Mol. Ther. *27*, 710–728.

STAR★METHODS

KEY RESOURCES TABLE

REAGENT or RESOURCE	SOURCE	IDENTIFIER
Antibodies		
Anti-TSG101	Proteintech	Cat# 28283-1-AP; RRID：AB_2881104
Anti-VDAC1	Proteintech	Cat# 55259-1-AP; RRID：AB_10837225
Anti-Flotillin 1	Proteintech	Cat# 15571-1-AP; RRID：AB_2106746
Anti-Wnt2	ABclonal	Cat# A23997; RRID:AB_3677320
Anti-CD47	ABclonal	Cat# A21904; RRID:AB_3677321
Anti-LYVE1	Invitrogen	Cat# 14-0443-82; RRID:AB_1633414
Anti-CLEC4F	Invitrogen	Cat# PA5-47396; RRID:AB_2608299
Anti-F4/80	Servicebio	Cat# GB113373-100; RRID: AB_3677324
Anti-LY6G	Proteintech	Cat# 65078-1-Ig; RRID：AB_2918382
Anti-Ki67	Servicebio	Cat# GB111141-100; RRID: AB_3677325
PE anti-mouse CD31	BioLegend	Cat# 102407; RRID：AB_312902
APC anti-mouse F4/80	BioLegend	Cat# 123115; RRID：AB_893493
Anti-Rabbit IgG H&L (HRP Conjugated)	ZENBIO	Cat# 511203; RRID:AB_2927753
Anti-Mouse IgG H&L (HRP Conjugated)	ZENBIO	Cat# 511103; RRID:AB_2893489
Donkey anti-Rat IgG H&L (Alexa Fluor 594)	Invitrogen	Cat# A21209; RRID:AB_2535795
Donkey anti-Rat IgG H&L (Alexa Fluor 488)	Invitrogen	Cat# A48269; RRID:AB_2893137
Donkey anti-Goat IgG H&L (Alexa Fluor 488)	Invitrogen	Cat# A32814; RRID:AB_2762838
Donkey anti-Rabbit IgG H&L (CY3)	Servicebio	Cat# GB21403; RRID:AB_2818951
Bacterial and virus strains		
CD47 overexpressing lentiviral vector	Hanbio	JY20230330ZY-LP01
Wnt2 overexpressing lentiviral vector	Hanbio	HH20230916ZY-LV01
Biological samples		
Liver Serum Primary liver sinusoidal endothelial cell Primary hepatocyte	Mice in this study	N/A
Chemicals, peptides, and recombinant proteins		
DMPE-PEG2000-CRLTRKRGLK	Ruixibio	R-DMK-0125
Acetaminophen	MCE	HY-66005
Dimethylnitrosamine	TCI	D0761
Puromycin, Sterile	MCE	HY-K1057
Blasticidin S, Sterile	MCE	HY-K1054
TRizol™	Invitrogen	15596026
Fetal bovine serum	BioInd	1706126
Dulbecco's Modified Eagle's Medium	Gibco	C11995500
DiI	Yeasen	40726ES10
DiO	Yeasen	40725ES10
TRITC Phalloidin	Yeasen	40734ES75
Cell Counting Kit-8	TargetMol	C0005
Critical commercial assays		
SYBR Green Pro Taq HS qPCR kit	Accurate Biology	11701
Mouse Protein Wnt-2 (WNT2) ELISA kit	CUSABIO	CSB-EL026133MO
One Step TUNEL Apoptosis Assay Kit	Beyotime	C1089
Mouse cluster of differentiation 47 (CD47) ELISA Kit	Jonlnbio	JL49445

(*Continued on next page*)

Continued

REAGENT or RESOURCE	SOURCE	IDENTIFIER
Deposited data		
RNA-seq data	This paper	SRA: PRJNA1213977
Experimental models: Cell lines		
bEnd.3	Cell Bank of the Chinese Academy of Science	SCSP-5267
RAW264.7	Cell Bank of the Chinese Academy of Science	SCSP-5036
293T	Cell Bank of the Chinese Academy of Science	GNHu17
Experimental models: Organisms/strains		
C57BL/6J	Charles River Laboratories	219
Oligonucleotides		
Primer used, see Table S1	Tsingke	N/A
Software and algorithms		
ImageJ	National Institutes of Health	https://imagej.nih.gov/ij/
Microsoft office	Microsoft	https://www.microsoft.com/zh
GraphPad Prism 10.0	GraphPad	http://www.graphpad-prism.cn/

EXPERIMENTAL MODEL AND STUDY PARTICIPANT DETAILS

Experimental mouse models and exosomes injection

8- to 10-week-old C57BL/6 mice (male) were purchased from Charles River Laboratories. All animal studies were approved by the Institutional Animal Care and Use Committee of the Fourth Military Medical University. For DMN-indued liver injury model, 10 μL/kg DMN (TCI, D0761) was intraperitoneal (i.p.) injected. Simultaneously, mice were randomly divided into three groups and were i.v. injected with PBS, Exo or RLTR-Wnt2@Exo^{CD47}. Mice were sacrificed at 48 h. Serum and liver tissues were collected for further analysis. For APAP-induced liver injury model, mice were given food and water from 6 p.m. to 9 p.m. in dark room and then fasted from 9 p.m. to 9 a.m. next day. 300 mg/kg APAP (MCE, HY-66005) was intraperitoneal (i.p.) injected, and food were given back. Meanwhile, mice were randomly divided into three groups and were i.v. injected with PBS, Exo or RLTR-Wnt2@Exo^{CD47}. Mice were sacrificed 36 h later. Serum and liver tissues were collected for further analysis.

Cell culture and transfection

All cell lines (HEK293T, bEnd.3, HUVEC and RAW 264.7) were obtained from the Cell Bank of the Chinese Academy of Sciences (Shanghai, China). Cells were cultured in complete media containing high glucose Dulbecco's modified Eagle medium (DMEM) with 10% fetal bovine serum and 1% penicillin/streptomycin in a humidified incubator with 5% CO_2 at 37°C. Cells were incubated at 37°C in a humidified atmosphere with 5% CO2. All cell lines were authenticated by STR profiling and tested for mycoplasma contamination using a specific PCR-based method prior to use. The authentication and mycoplasma testing services were provided by the CAS Cell Bank to ensure the identity and purity of the cell lines.

The CD47 overexpressing lentiviral vector and the negative control vector were purchased from Shanghai hanbio company, and cocultured with bEnd.3 cells at 37°C for 48 h, respectively. The fluorescence from ZsGreen was observed under fluorescence microscope after transfection. The transfection results were verified by RT-qPCR and western blotting (WB). After confirming the fluorescence intensity of lentivirus in the cells, the cells were seeded into T25 culture flasks, and screened with 5 μg/mL of puromycin (MCE, HY-K1057) for 72 h. Afterward, the medium was replaced, and the cells continued to be cultured in the incubator. The bEnd.3 cells with stable overexpression of CD47 (CD47^{OE}-bEnd.3) was prepared. The preparation of bEnd.3 cells with stable overexpression of CD47 and Wnt2 (CD47^{OE}&Wnt2^{OE}-bEnd.3), was similar to the above.

METHOD DETAILS

Exosome isolation and labeling

Cells were cultured in high-glucose Dulbecco's modified Eagle medium (DMEM) supplemented with 10% fetal bovine serum and 1% penicillin/streptomycin, in a humidified incubator at 5% CO_2 at 37°C. When the cells confluence reached 90%, the previous medium was replaced by that with DMEM without fetal bovine serum. After 48–72 h, the supernatant was harvested for gradient centrifugation and finally exosomes were obtained. The supernatant underwent 2000 × g centrifugation (5 min), 10000 × g centrifugation (1 h), and 110000 × g ultracentrifugation (70 min) to collect the sediment at last. Then the sediment was resuspended with 1 mL PBS and

underwent 110000 × g ultracentrifugation (70 min) for washing to obtain exosomes in the sediment, which was resuspended in 100 μL PBS. The exosomes were stored at −80°C within 30 days for the following experiments. For labeling, exosomes in PBS were incubated with DiI/DiO (Yeasen Biotechnology) at 37°C for 30 min, and then washing twice at 120000 × g for 30 min to remove free fluorescence dye.

Synthesis of DMPE-PEG2000-CRLTRKRGLK

DMPE-PEG2000-CRLTRKRGLK was synthesized via the reaction between thiol group and maleimide (Mal) functional group. Specifically, 100 mg of DMPE-PEG2000-Mal was dissolved in 5 mL of anhydrous N,N-dimethylformamide (DMF) under nitrogen atmosphere. Subsequently, 1.1 equivalents (eq) of the peptide CRLTRKRGLK were added, and the reaction mixture was stirred at 25°C for 12 h. The crude product was purified by dialysis using a membrane with a molecular weight cutoff (MWCO) of 2000 Da against ultrapure water (24 h, 4°C). The retentate was collected and lyophilized to obtain DMPE-PEG2000-CRLTRKRGLK as a white powder. To determine the chemical structure, both CRLTRKRGLK and DMPE-PEG2000-CRLTRKRGLK were dissolved in D_2O and then detected by ^{1}H-NMR spectroscopy operating at 400 MHz, 25°C.

Preparation and characterization of RLTR-Exo

For exosomes modification, Exo (200 μg/mL) and DMPE-PEG2000-CRLTRKRGLK (30 μM) were gently mixed and incubated in PBS buffer at 40°C for 1 h. Afterward, free DMPE-PEG2000-CRLTRKRGLK was removed through centrifuging twice. The size distribution of the exosomes before and after RLTR surface modification was analyzed by flow cytometry for nanoparticle analysis (NanoFCM, Xiamen, China) and exosomes morphology was observed by TEM.

Isolation of primary hepatic cells

Mice were anesthetized and perfused through inferior vena cava with Hank's buffer containing 0.2 mg/mL of collagenase IV (Sigma-Aldrich). Primary hepatocytes were collected by low-speed centrifugation at 50 × g for 3 min. Liver NPCs were resuspended in 4 mL of 17.6% iodixanol (Axis-Shield, Dundee, Scotland) and 4 mL of 10% iodixanol. The cell suspension then was centrifuged at 1400 × g for 21 min in a swingout rotor without brake. Cells were collected from the interface between the 10% and 17.6% iodixanol solutions, resuspended and incubated with anti-CD146 magnetic beads (Miltenyi Biotec) for 30 min in the dark at 4°C. By magnetic separation with MS Columns (Bergisch Gladbach, Germany), LSEC were collected by pushing the plunger into the MS column.

Western blotting

Total proteins from samples (cells, exosomes, and tissue) were extracted at 4°C for 30 min by using RIPA Lysis Buffer (Beyotime, China). Then, the lysates were centrifuged at 12000 rpm for 10 min at 4°C and the supernatant was collected. Western blotting was performed according to the concentration of proteins determined by BCA method. The protein samples were analyzed by sodium dodecyl sulfate (SDS)–PAGE, transferred to polyvinylidene fluoride membranes (Millipore, Billerica, MA, USA), and incubated first with primary antibodies and then with HRP-conjugated goat anti-mouse or anti-rabbit IgG secondary antibodies.

In vivo biodistribution study

For *in vivo* exosome tracking, mice were injected with fluorescent dye-labelled exosomes via the tail vein. The mice were sacrificed at the scheduled time point post-injection, and the main organs (including heart, liver, spleen, lung, and kidney) were harvested. The fluorescence radiation efficiency of the organs was measured by the imaging system (IVIS Spectrum system, PerkinElmer, USA). The excitation and emission filters depended on the fluorescent dye used for labeling exosomes.

For immunofluorescence imaging, main organs from mice that received fluorescent dye-labelled exosomes were fixed with 4% paraformaldehyde and then sliced. After blocking, the LSEC in liver was stained with LYVE1 (Invitrogen, 14-0443-82), the KC was stained with F4/80 (Servicebio, GB113373-100), and the nuclei was stained with DAPI. The fluorescent signals of the samples were analyzed by fluorescence microscope. More importantly, the specific cellular internalization of exosomes in liver was visualized using confocal microscopy.

We further analyzed the cellular distribution of DiO-labelled exosomes in LSEC/KC using flow cytometry. Mice were injected with DiO-labelled exosomes, NPCs were isolated via liver pronase-collagenase prefusion 12 h later. NPCs were stained with PE anti-mouse CD31 antibody (BioLegend, 102407) and APC anti-mouse F4/80 antibody (BioLegend, 123115). KCs were identified using F4/80 labeling, while ECs were identified using CD31 labeling. Prepared samples were then analyzed by flow cytometry (SONY MA900).

In vitro cellular uptake study

For the cellular uptake of exosomes *in vitro*, cells were seeded in cover glass (Servicebio) at a density of cell loading tailored to experimental requirements. Cultured overnight in an atmosphere of 5% CO_2 at 37°C, cells were then incubated with prepared fluorescent dye-labelled exosomes for a specified duration. To observe cellular uptake and internalization of exosomes by cells, the cells on the cover glass were washed three times with 1 × PBS and fixed with 4% paraformaldehyde (Servicebio) for 30 min. Subsequently, the cell F-actin was stained with TRITC Phalloidin (Yeasen Biotechnology), and the cell nuclei were stained with DAPI (Servicebio) for 10 min. Finally, the fluorescence signals of the labelled-exosomes were imaged by confocal microscopy.

Evaluation of liver injury

Paraffin-embedded and snap-frozen liver sections were prepared for immunohistochemistry and immunofluorescence according to standard protocols. Hematoxylin–eosin (H&E) staining was implemented to roughly quantify the area of the necrotic areas. TUNEL staining was used to count cell death. And the inflammatory infiltration was evaluated by immunofluorescence of LY6G, and double-staining with CLEC4F and F4/80.

Serum albumin (ALB), alanine aminotransferase (ALT), aspartate aminotransferase (AST), and total bilirubin (TBIL) levels were determined using an automatic biochemical analyzer (Rayto Life and Analytical Sciences Company, Shenzhen, China).

Cytotoxicity evaluation

To assess the cytotoxicity of RLTR-Wnt2@Exo^{CD47}, bEnd.3 cells were counted and then seeded in 96-well plates. After overnight culture, cells were incubated with different concentrations of Exo and RLTR-Wnt2@Exo^{CD47}. Cell viability was determined using Cell Counting Kit-8 (TargetMol, C0005) assay at 12 h, 24 h, and 48 h after incubation. Cell Counting Kit-8 working solution was added to each well and incubated at 37°C for 2 h, and quantified at 450 nm with an EPOCH microplate spectrophotometer reader (Agilent BioTek).

In vivo toxicity study

Mice were injected through the tail vein with PBS (as control), Exo, and RLTR-Wnt2@Exo^{CD47}. 48 h after injection, blood was collected and then the serum was separated by 3000 g, 5 min centrifuge, which was used to detect ALT, AST, BUN, CREA, LDH and LDH1. After the mice were sacrificed by cervical dislocation, important organs (including heart, liver, spleen, lung, and kidney) from these mice were sectioned for H&E staining and subsequent examination under a light microscope.

QUANTIFICATION AND STATISTICAL ANALYSIS

All data were expressed as the mean ± standard deviation (SD). Statistical analysis was performed with GraphPad Prism 10 (GraphPad Software, San Diego, CA, USA). Statistical comparison between two groups was done with the unpaired Student's t test. Multiple-group comparison was done with One-Way ANOVA. The statistical details for each experiment can be found in the figure legends. $p < 0.05$ was considered statistically significant. $^{*}p < 0.05$, $^{**}p < 0.01$, and $^{***}p < 0.001$, $^{****}p < 0.0001$.

Cell Reports Medicine, Volume *6*

Supplemental information

A combined “eat me/don't eat me” strategy based on exosome for acute liver injury treatment

Wei Du, Chen Chen, YingYing Liu, Huiyi Quan, Ming Xu, JingJing Liu, Ping Song, ZhiQiang Fang, ZhenSheng Yue, Hao Xu, YuWei Ling, JuanLi Duan, Fei He, and Lin Wang

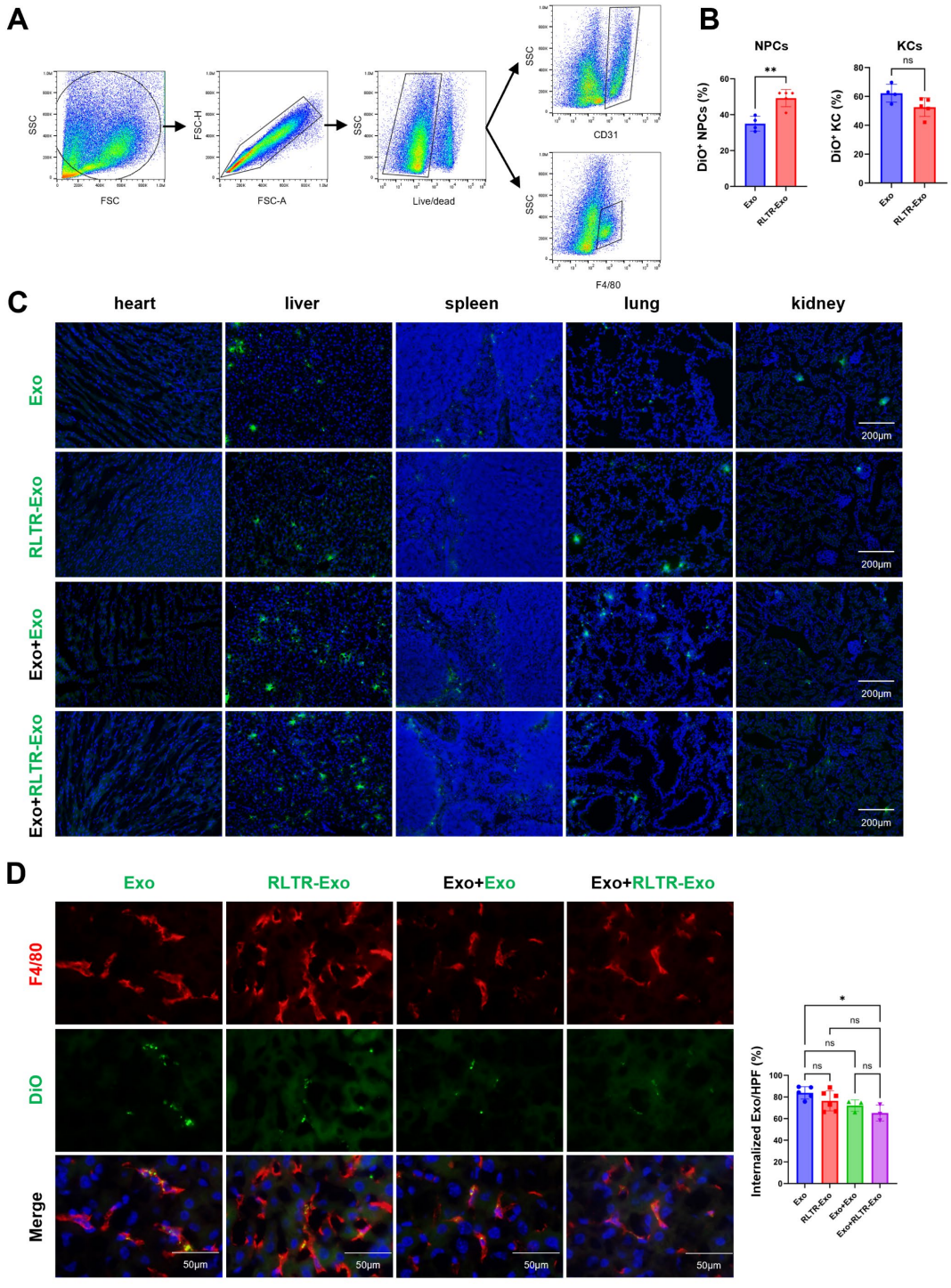

Figure S1. Biodistribution of DiO-labelled exosomes *in vivo.* Related to Figure 2.

(A) Gating strategies to distinguish the NPCs. The cells were pre-gated on single cells and live cells. LSECs were defined as $CD31^+$ cells and KCs as $F4/80^+$ cells.

(B) FCM analysis of $FITC^+$ NPCs (left) and KCs (right) ratio after administration intravenously with DiO-labelled Exo and RLTR-Exo. Exo: n=4, RLTR-Exo: n=5.

(C) Immunofluorescence analysis of the biodistribution of exosomes in major organs with different injection strategies. Green: DiO labelled Exo and RLTR-Exo. Blue: DAPI labelled nuclei. Scale bar:

200 μm.

(D) Immunofluorescence of liver collected from mice with different injection strategies showing the cellular uptake and internalization of exosomes by KC. Red: F4/80. Green: DiO labelled Exo and RLTR-Exo. Blue: DAPI labelled nuclei. Exo: n=5, RLTR-Exo: n=6, Exo + Exo: n=3, Exo + RLTR-Exo: n=3. Scale bar: 50 μm.

Data are represented as mean ± SD (error bars) from biological replicates. Statistical analyses, n.s., not significant, * $P < 0.05$, ** $P < 0.01$. Statistical significance was determined by unpaired Student's t test or one-way ANOVA where appropriate.

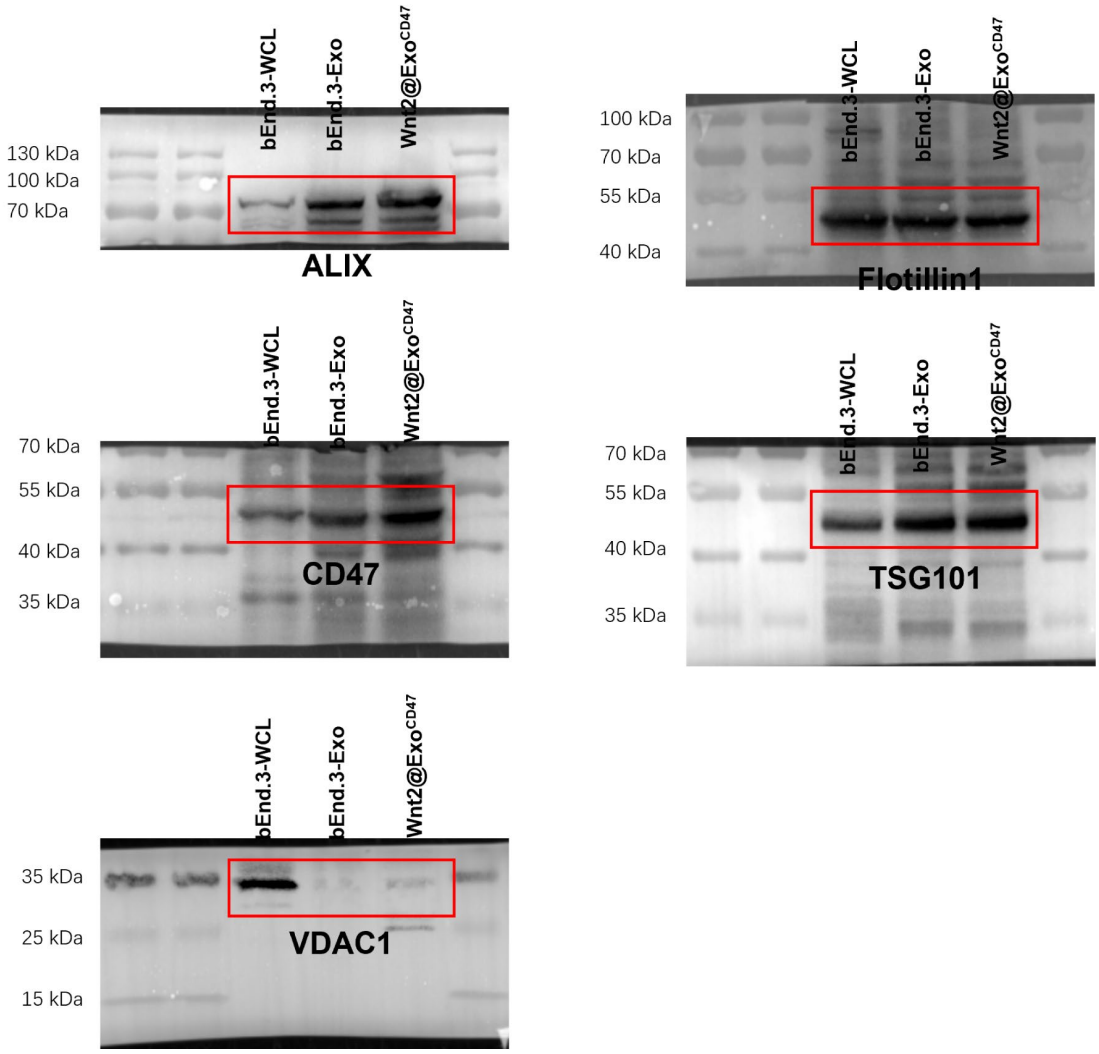

Figure S2. The original uncropped images of western blot in Figure 3. Related to Figure 3.

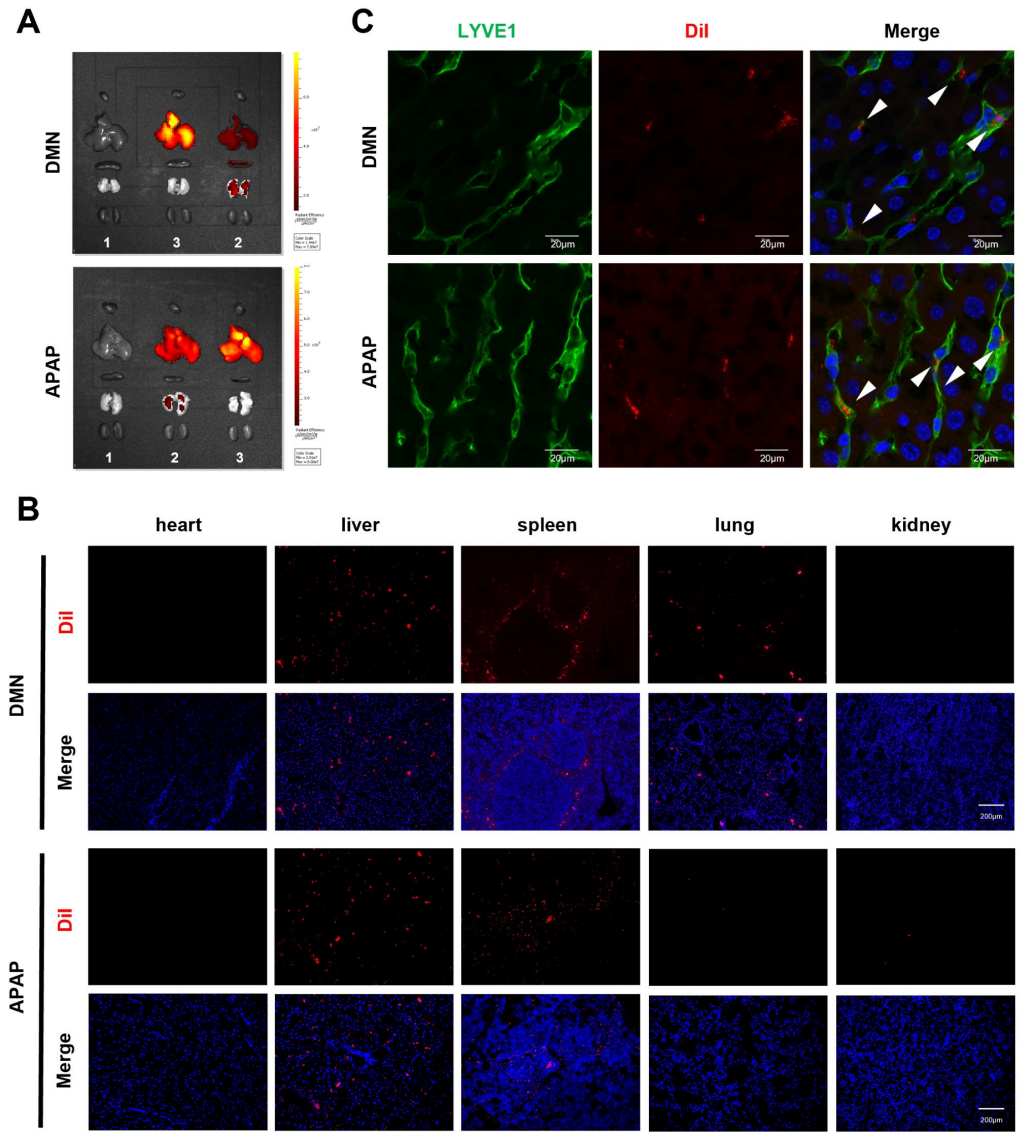

Figure S3. Biodistribution of RLTR-Wnt2@Exo^{CD47} in DMN/APAP induced liver injury mice *in vivo*. Related to Figure 5.

(A) *ex vivo* fluorescence image of main organs at 12 h post-injection intravenously with Exo (1), DiI-labelled Exo (2), or DiI-labelled RLTR-Wnt2@Exo^{CD47} (3). Exosomes were stained with Dil and approximately 200 μg (protein equivalent) of exosomes in 200 μL of PBS were injected into mice with DMN/APAP-induced liver injury via the tail vein.

(B) Immunofluorescence staining of main organs collected from DMN/APAP model mice at 12 h post-injection intravenously with DiI-labelled RLTR-Wnt2@Exo^{CD47}. Red: DiI-labelled RLTR-Wnt2@Exo^{CD47}. Blue: DAPI labelled nuclei. Scale bar: 200 μm.

(C) CLSM images of liver section showing internalization of DiI-labelled RLTR-Wnt2@Exo^{CD47} by LSEC in DMN/APAP mice. Red: DiI-labelled RLTR-Wnt2@Exo^{CD47}. Green: LYVE1. Blue: DAPI labelled nuclei. Scale bar: 20 μm.

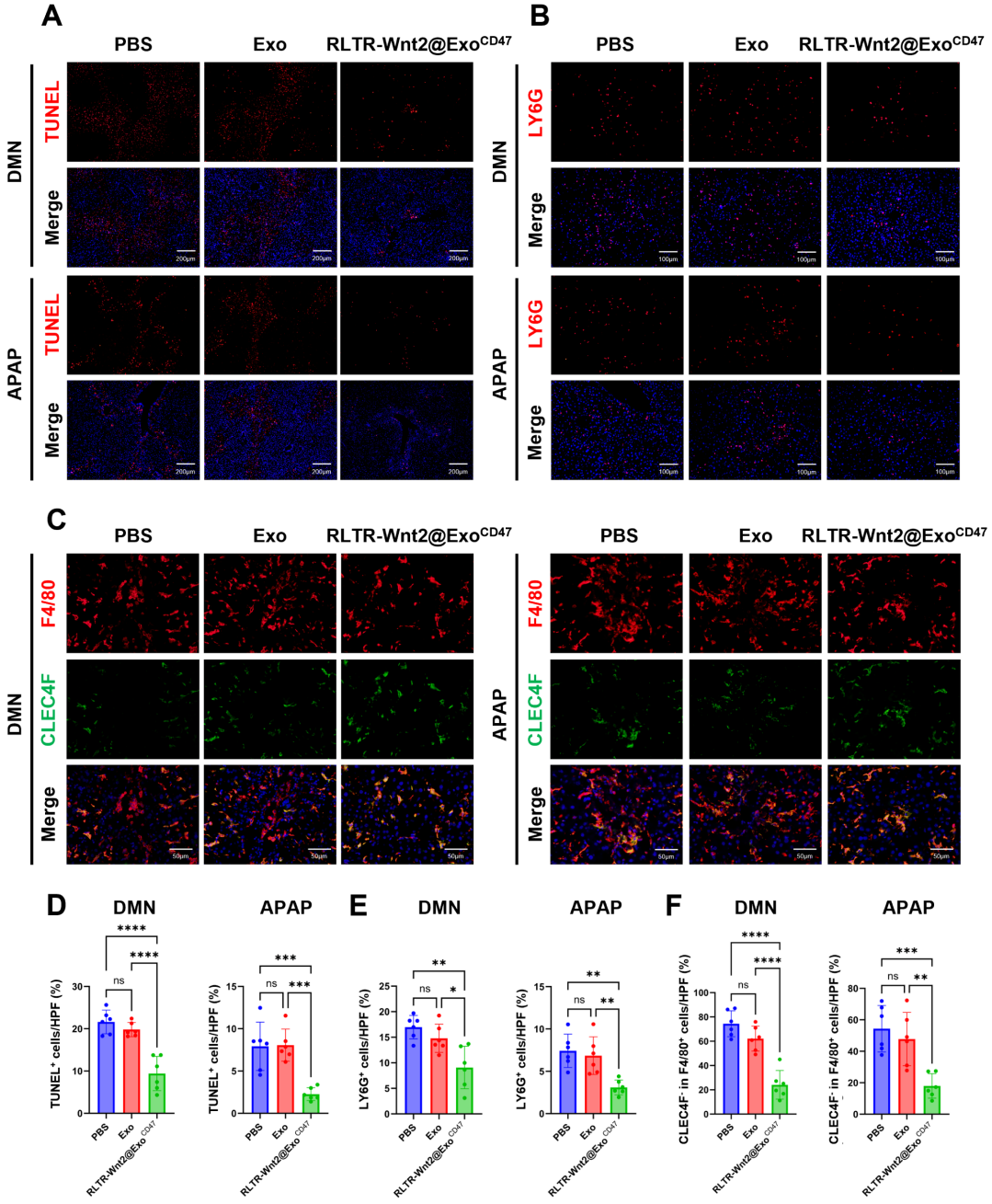

Figure S4. Histological analysis of APAP and DMN acute liver injury mice across different treatment group. Related to Figure 5.

(A) TUNEL staining of liver tissue in DMN (up) and APAP (down) liver injury mice treated with PBS, Exo, or RLTR-Wnt2@Exo^{CD47}. Red: TUNEL. Blue: DAPI labelled nuclei. n=6. Scale bar: 200 μm.

(B) LY6G staining of liver tissue in DMN (up) and APAP (down) liver injury mice treated with PBS, Exo, or RLTR-Wnt2@Exo^{CD47}. Red: LY6G. Blue: DAPI labelled nuclei. n=6. Scale bar: 100 μm.

(C) F4/80 and CLEC4F double staining of liver tissue in DMN and APAP liver injury mice treated with PBS, Exo, or RLTR-Wnt2@Exo^{CD47}. Red: F4/80. Green: CLEC4F. Blue: DAPI labelled nuclei. n=6. Scale bar: 50 μm.

(D) Statistical analysis of TUNEL^{+} cells in A. n=6.

(E) Statistical analysis of LY6G^{+} cells in B. n=6.

(F) Statistical analysis of CLEC4F^{-} F4/80^{+} cells in C. n=6.

Data are represented as mean ± SD (error bars) from biological replicates. Statistical analyses, n.s., not significant, * $P < 0.05$, ** $P < 0.01$, *** $P < 0.001$, **** $P < 0.0001$. Statistical significance was determined by one-way ANOVA.

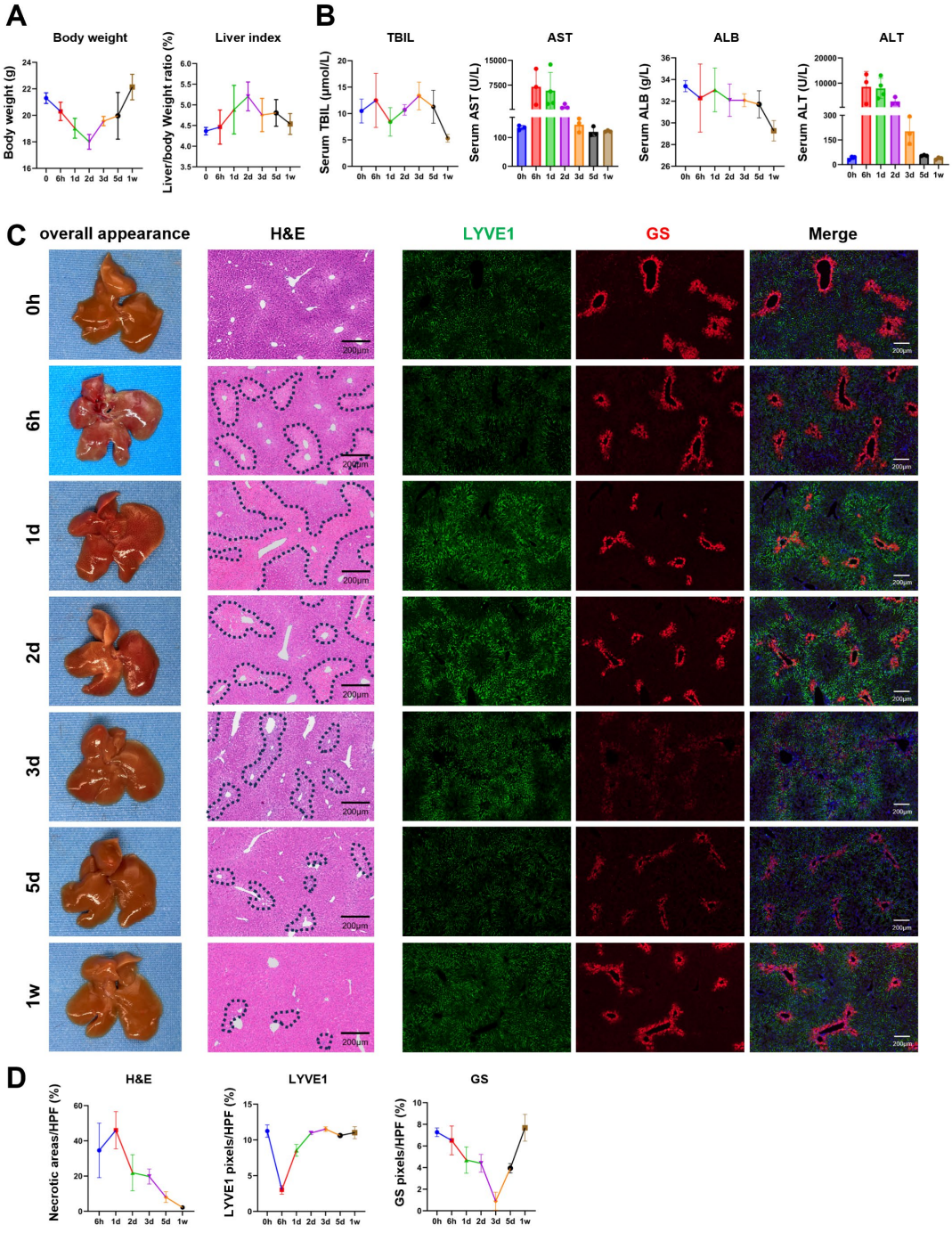

Figure S5. Analysis of APAP-induced acute liver injury mice model without therapeutic interventions. Related to Figure 5.

(A) The body weight and liver/body weight ratio at different time points after exposure to APAP. n=3.

(B) Serum ASL, ALT, ALB, and TBIL at different time point after exposure to APAP. n=3. ALB: albumin, ALT: alanine aminotransferase, AST: aspartate aminotransferase, TBIL: total bilirubin.

(C) Overall appearance, H&E staining, and immunofluorescence co-staining with LYVE1 and GS of liver from APAP injured mice. Red: GS. Green: LYVE1. Blue: DAPI labelled nuclei. n=3. Scale bar: 200 μm.

(D) Quantitative analysis of the liver histological staining at different time points as shown in C,

including necrotic areas, GS, and LYVE1 expression. Time point: 0 h, 6 h, 1 d, 2 d, 3 d, 5 d, and 1 w after APAP induced liver injury.
Data are represented as mean ± SD (error bars) from biological replicates.

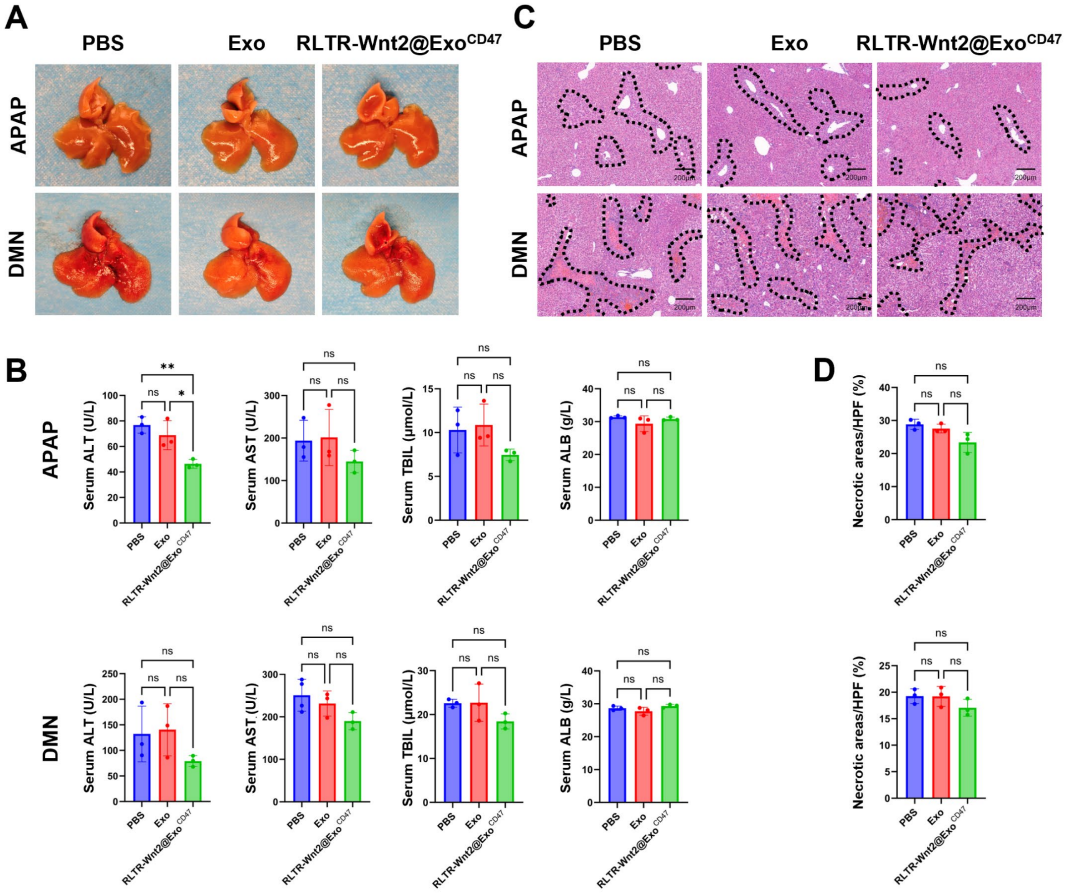

Figure S6. The delayed administration of engineered exosomes shows limited efficacy in treating acute liver injury mice. Related to Figure 5.

(A) The overall appearance of the livers in mice administration with PBS, Exo or RLTR-Wnt2@Exo^{CD47} after APAP (up) and DMN (down) induced liver injury.

(B) Serum ALT, AST, ALB, and TBIL of mice administration with PBS, Exo or RLTR-Wnt2@Exo^{CD47} post APAP/DMN liver injury. n=3. ALB: albumin, ALT: alanine aminotransferase, AST: aspartate aminotransferase, TBIL: total bilirubin.

(C) H&E staining of liver sections from mice treated with PBS, Exo or RLTR-Wnt2@Exo^{CD47} after APAP (up) and DMN (down) induced liver injury. Scale bar: 200 μm.

(D) Statistical analysis of liver necrotic areas in C. n=3.

Data are represented as mean ± SD (error bars) from biological replicates. Statistical analyses, n.s., not significant, * $P < 0.05$, ** $P < 0.01$. Statistical significance was determined by one-way ANOVA.

Gene name	Sequences (5’-3’)	
CD47	Forward	TGCGGTTCAGCTCAACTACTG
	Reverse	ACGATGCAAGGGATGACCAC
Mki67	Forward	ATCATTGACCGCTCCTTTAGGT
	Reverse	GCTCGCCTTGATGGTTCCT
Wnt2	Forward	CCTCCGAAGTAGTCGGGAATC
	Reverse	GCAGGACTTTAATTCTCCTTGGC
Ccnd1	Forward	GCGTACCCTGACACCAATCTC
	Reverse	ACTTGAAGTAAGATACGGAGGGC
Actb	Forward	GGCTGTATTCCCCTCCATCG
	Reverse	CCAGTTGGTAACAATGCCATGT
Axin2	Forward	AACCTATGCCCGTTTCCTCTA
	Reverse	GAGTGTAAAGACTTGGTCCACC
Birc5	Forward	CTACCGAGAACGAGCCTGATT
	Reverse	AGCCTTCCAATTCCTTAAAGCAG
Myc	Forward	CCCTATTTCATCTGCGACGAG
	Reverse	GAGAAGGACGTAGCGACCG

Table S1. Primer sequences. Related to STAR Methods.

The information of primers applied, including gene name and sequencings of forward/reverse (5'-3') primers.